Predictability and Dynamics of Hurricane Joaquin (2015) Explored through Convection-Permitting Ensemble Sensitivity Experiments

ROBERT G. NYSTROM,[a] FUQING ZHANG,[a] ERIN B. MUNSELL,[b,c] SCOTT A. BRAUN,[b] JASON A. SIPPEL,[d] YONGHUI WENG,[a,e] AND KERRY EMANUEL[f]

[a] *Department of Meteorology and Atmospheric Science, and Center for Advanced Data Assimilation and Predictability Techniques, The Pennsylvania State University, University Park, Pennsylvania*
[b] *NASA Goddard Space Flight Center, Greenbelt, Maryland*
[c] *Universities Space Research Association, Columbia, Maryland*
[d] *NOAA/Atlantic Oceanographic and Meteorological Laboratory/Hurricane Research Division, Miami, Florida*
[e] *I. M. System Group, Rockville, Maryland*
[f] *Lorenz Center, Massachusetts Institute of Technology, Cambridge, Massachusetts*

(Manuscript received 1 May 2017, in final form 31 October 2017)

ABSTRACT

Real-time ensemble forecasts from the Pennsylvania State University (PSU) WRF EnKF system (APSU) for Hurricane Joaquin (2015) are examined in this study. The ensemble forecasts, from early in Joaquin's life cycle, displayed large track spread, with nearly half of the ensemble members tracking Joaquin toward the U.S. East Coast and the other half tracking Joaquin out to sea. The ensemble forecasts also displayed large intensity spread, with many of the members developing into major hurricanes and other ensemble members not intensifying at all.

Initial condition differences from the regions greater than (less than) 300 km were isolated by effectively removing initial condition differences in desired regions through relaxing each ensemble member to GFS (APSU) initial conditions. The regions of initial condition errors contributing to the track spread were examined, and the dominant source of track errors arose from the region greater than 300 km from the tropical cyclone center. Further examination of the track divergence revealed that the region between 600 and 900 km from the initial position of Joaquin was found to be the largest source of initial condition errors that contributed to this divergence. Small differences in the low-level steering flow, originating from perturbations between 600 and 900 km from the initial position, appear to have resulted in the bifurcation of the forecast tracks of Joaquin. The initial condition errors north of the initial position of Joaquin were also shown to contribute most significantly to the track divergence. The region inside of 300 km, specifically, the initial intensity of Joaquin, was the dominant source of initial condition errors contributing to the intensity spread.

1. Introduction

Tropical cyclone (TC) track forecasts have improved substantially over the past few decades. The 48-h track errors in the North Atlantic today have been reduced by 50% over the last 15 years (Cangialosi and Franklin 2016). While these improvements in the forecast tracks generally hold, Hurricane Joaquin (2015) presents an unusual case in which current numerical weather prediction models struggled with the track forecast. The initial poor track forecast of Joaquin resulted in false alarms along the eastern seaboard of the United States as a hurricane that was initially forecasted to make landfall, in reality, stayed out at sea.

Berg (2016) described the full life cycle of Joaquin. Instead of developing from an African easterly wave, the common initial source of major hurricanes in the North Atlantic (Landsea 1993), Joaquin developed from an upper-level low pressure system. Joaquin became a tropical storm by 0000 UTC 29 September to the north-northeast of the Bahamas. At 1200 UTC 29 September, the initial time for the ensemble forecast examined in this study, Joaquin was a tropical storm with an initial intensity of 45 kt (1 kt = 0.51 m s^{-1}) and was located to the north-northeast of the Bahamas (Fig. 1a). Also at this time, an upper-level trough important in the genesis of Joaquin was located to the

Corresponding author: Professor Fuqing Zhang, fzhang@psu.edu

DOI: 10.1175/JAS-D-17-0137.1

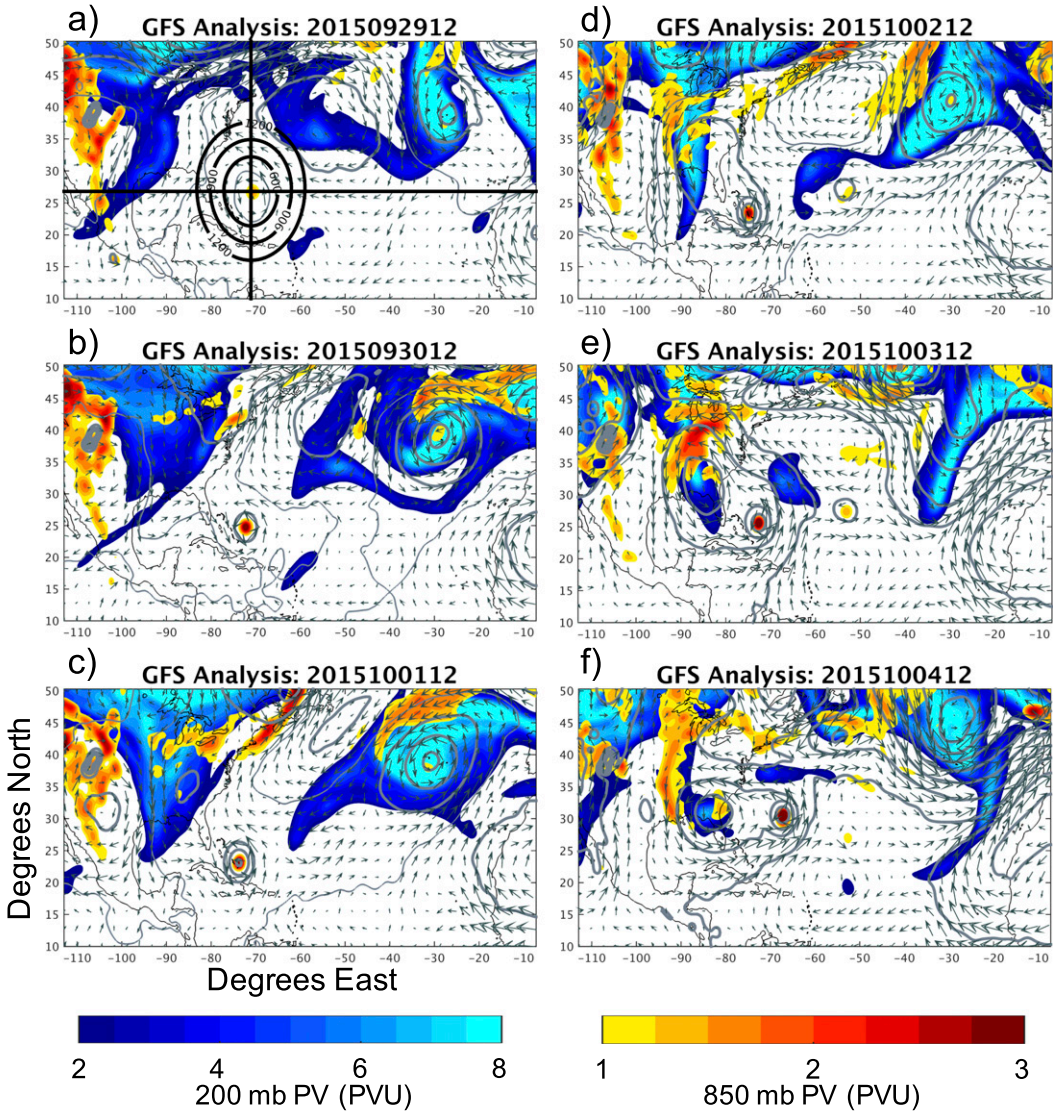

FIG. 1. Large-scale GFS analysis of 200-hPa PV (cool colors), 850-hPa PV (warm colors), 700-hPa winds (vectors), and 700-hPa geopotential height (contoured every 50 m) every 24 h between 1200 UTC 29 Sep and 1200 UTC 4 Oct. Rings shown at 1200 UTC 29 Sep highlight radii of 600, 900, and 1200 km from initial center location, and vertical (horizontal) lines highlight regions east–west (north–south) of initial storm location.

northeast of Joaquin while a midlatitude trough was located over the central United States. Over the next 72 h (1200 UTC 29 September–1200 UTC 2 October), Joaquin tracked south-southwestward into the Bahamas while it rapidly intensified into a major hurricane (reaching hurricane intensity by 0000 UTC 1 October) (Figs. 1a–d). During this time, the low over the southeastern United States strengthened, and a low- to mid-level low intensified to the east of Joaquin, which likely helped to steer Joaquin to the south-southwest. Joaquin devastated the Bahamas for nearly 2 days as its forward motion slowed before eventually turning clockwise and heading into the northern Atlantic. While Joaquin's motion slowed in the Bahamas, historic flooding commenced along the eastern coast of the United States when a cutoff low pressure system developed over the southeastern United States and transported moisture from Joaquin into the region. By 1200 UTC 3 October, Joaquin had turned northward and began to track to the northeast, away from the U.S. coast (Fig. 1e). The westerly winds in the southern region of the low pressure system located over the southeastern United States

helped steer Joaquin farther east initially and then to the northeast as Joaquin was located well to the east of the United States by 1200 UTC 4 October (Fig. 1f).

The forecasts for the track of Joaquin were uncharacteristically poor. The 72–120-h track errors were more than double the mean track errors over the previous 5 years. These errors likely resulted from the unusual southwestward motion of Joaquin following tropical cyclogenesis (Berg 2016). Both deterministic and ensemble forecasting systems struggled to accurately or confidently forecast the track of Joaquin. Official National Hurricane Center (NHC) intensity forecast errors between 72 and 96 h were ~70% larger than intensity errors over the previous 5 years. These poor/uncertain forecasts may have contributed to the loss of the *El Faro*, a rare loss of such a large ship.

The need for ensemble forecasting of TCs as a result of rapid initial condition (IC) error growth has been discussed thoroughly in the literature for both track (e.g., Zhang and Krishnamurti 1997; Cheung and Chan 1999a,b; Chan and Li 2005; Komaromi et al. 2011; Magnusson et al. 2014) and intensity forecasts (e.g., Zhang and Sippel 2009; Sippel and Zhang 2010; Torn and Cook 2013; Zhang and Tao 2013; Tao and Zhang 2014, 2015; Komaromi and Majumdar 2014; Torn 2016; Rios-Berrios and Torn 2016). In addition to providing forecasters with means through which to access the confidence of a forecast and helping improve track forecasts through ensemble-based data assimilation methods (e.g., Hamill et al. 2011; Weng and Zhang 2012), ensemble forecasts can be used to better understand forecast sensitivity to ICs. For example, Munsell and Zhang (2014) examined the divergence in the ensemble track forecasts of Hurricane Sandy (2012) and found that uncertainties in the tropical flow led to the ensemble track divergence. Magnusson et al. (2014) examined ECMWF ensemble forecasts of Hurricane Sandy and found that the forecasted landfall was not sensitive to horizontal resolution of the model and instead related to differences in the subtropical ridge strength. Torn et al. (2015) and Bassill (2015) also examined the bifurcation in the forecast tracks of Sandy and suggested that the ridge amplification was important in explaining the cause of forecast divergence and may have resulted from the entrainment coefficient in the cumulus parameterization. Additionally, while it is well accepted that the environment largely determines the motion of TCs (George and Gray 1976; Dong and Neumann 1986; Fiorino and Elsberry 1989; Cheung and Chan 1999a; Chan 2005), it is not completely understood how and in what regions the environmental IC differences most influence TC track forecasts.

Output from the real-time Pennsylvania State University Weather Research and Forecasting Model coupled with an ensemble Kalman filter (PSU WRF EnKF) for Joaquin is utilized for this study (Weng and Zhang 2016; Zhang and Weng 2015). The 60-member ensemble from 1200 UTC 29 September 2015 produced a bifurcated track forecast with nearly half of the members making landfall along the East Coast of the United States and half heading out to sea. The ensemble also produced large intensity spread, with many members developing into major hurricanes and others not intensifying at all. This initialization time is representative of track and intensity forecast uncertainty in the PSU WRF ENKF over an extended period (28 September–1 October). This time also coincides with large track and intensity forecast errors from multiple operational NWP models and NHC official forecasts. The purpose of this study is to understand the reasons for the large track and intensity spread in the ensemble forecasts of Joaquin and identify potential regions of IC errors that contributed to the track bifurcation and large intensity spread.

Section 2 will describe the methods used in this study, including the details of the PSU WRF EnKF system. Section 3 will examine the regions of IC errors contributing to the track and intensity spread. Section 4 will provide a summary of the main conclusions.

2. Methods

a. PSU WRF EnKF system

The 60-member PSU WRF EnKF real-time initialization from 1200 UTC 29 September is used to run a 126-h forecast of Joaquin. The deterministic forecast from the PSU WRF EnKF is initialized from the EnKF analysis mean. The 60 ensemble members are produced by the 3-h-cycling PSU WRF EnKF hurricane analysis and forecast system (Weng and Zhang 2016), and the initial perturbations for the first cycle (0000 UTC 28 September) are generated using the background error covariance discussed in Barker et al. (2004). The configuration of the 2016 PSU real-time cycling WRF EnKF system is the same as introduced in Weng and Zhang (2016); it is unique in that, in addition to conventional observations, it is capable of assimilating airborne Doppler radar observations (Weng and Zhang 2012) from the NOAA P-3 and G-IV aircraft (Gamache et al. 1995) and sounding observations (Munsell et al. 2017), though no airborne Doppler radar observations were available before the initialization for the ensemble discussed in this study. The PSU WRF EnKF utilizes WRF, version 3.5.1 (Skamarock et al. 2008), and contains three two-way nested

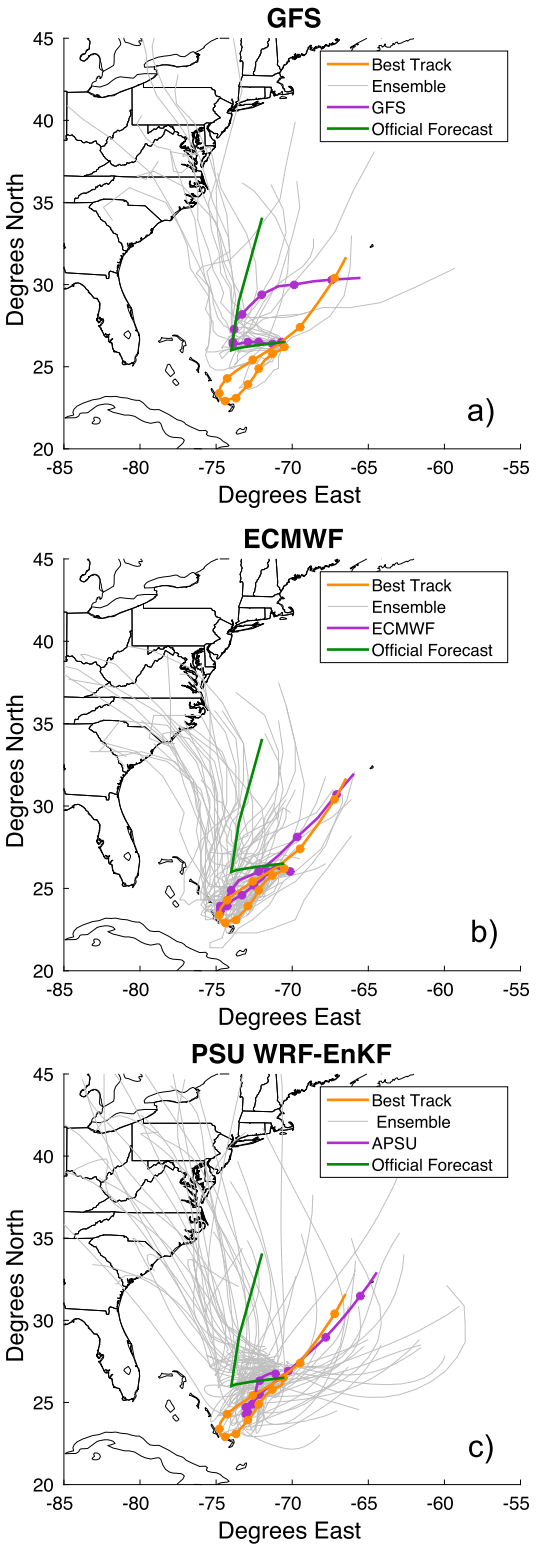

FIG. 2. Real-time ensemble and deterministic 126-h track forecasts from 1200 UTC 29 Sep from (a) GFS, (b) ECMWF, and (c) PSU WRF EnKF. The best track during this time period is also shown along with the official forecast from the NHC issued at 1500 UTC 29 Sep. Markers on deterministic forecasts and best track denote location every 12 h.

domains with horizontal grid spacing of 27, 9, and 3 km. Domain configuration and parameterization schemes are identical to those described by Zhang and Weng (2015). The boundary conditions for the outermost domain are provided by the operational Global Forecast System (GFS) forecast closest in time to the initialization time and are identical for all ensemble members in this study.

The PSU WRF EnKF ensemble has IC perturbations from the mean in both the storm inner-core region (within 300 km from the center) and the environment (beyond 300 km from the storm center). The region greater than 300 km from the best-track center is gradually relaxed to the deterministic GFS between 300 and 600 km in the WRF EnKF mean using a linear combination of the GFS and WRF EnKF mean such that, beyond 600 km from the storm center, the environment is identical to GFS. This is done every 6 h in the PSU WRF EnKF system because no observations are assimilated in this region to constrain the uncertainty. The ensemble members are then perturbed from the WRF EnKF mean in the environment using the background error covariance method (Barker et al. 2004). Because the perturbations in the inner-core region (within 300 km) and in the environment (outside 600 km) are constructed separately, the effects of the IC perturbations from each of these regions can be isolated and their influence on the track and intensity forecast spread examined. The process of removing the IC differences in a specific region is referred to throughout this manuscript as relaxing. A strength of this technique is that it illustrates the effects of IC differences only within a specific region and can help to more clearly understand how IC differences within a specific region evolve and ultimately cause forecast differences. A weakness of this technique is that it removes any potential nonlinear interactions of IC differences in two regions when the IC differences have been removed from one of the regions by relaxation. Another potential weakness is that perturbations to the vortex and the environment are not consistent with each other. There are no issues with struggling to spin up the vortex of Joaquin created through this relaxation method, although it could be an issue if a very small relaxation radius is chosen that disrupts the inner-core structure significantly.

b. Steering flow

In this study, the steering flow is calculated using an iterative method that makes no assumptions for which radii the steering flow should be calculated within or what vertical levels should be averaged (Galarneau and Davis 2013). This method will be referred to as the

optimal steering flow. The TC vorticity and divergence are first removed within a certain distance (from 1° to 8° every 1° are tested) by subtracting the nondivergent and irrotational wind from the total wind. This resulting wind field is then averaged within the specified radii at each level. Different vertical mean depths are tested between (850 and 200 hPa every 50 hPa). This results in 104 different calculations for the steering flow, and the vector difference between each of these and the actual storm motion, defined as the 6-h storm motion centered on each time, is computed. The optimal steering flow is considered to be the combination with the lowest error when compared to the actual motion.

3. Results and discussion

a. Examination of real-time ensembles

While the official forecast track errors of Hurricane Joaquin were larger than average, the PSU WRF EnKF, ECMWF, and GFS deterministic forecasts from 1200 UTC 29 September did correctly forecast Joaquin turning out to sea despite some forecasts (GFS especially) still having large errors in the initial motion (Fig. 2). The GFS deterministic and ensemble forecasts struggled to accurately capture the initial southwestward motion of Joaquin toward the Bahamas, where Joaquin caused the majority of its destruction. The PSU WRF EnKF deterministic (hereafter, APSU) and ensemble forecasts also struggled, although less than the GFS, to track Joaquin as far toward the south-southwest and into the Bahamas. The ECMWF ensemble and deterministic forecasts better captured the extent of the initial southwestward motion of Joaquin.

While the deterministic forecasts from each system correctly forecasted Joaquin turning away from the United States, the associated ensemble members from each of these forecasting systems contained large spreads in the track, and the initial southwestward motion was poorly forecasted. The NHC noted this large uncertainty and even mentioned the uncertainty in their forecast discussion from 1500 UTC 29 September, acknowledging that "confidence in the track forecast is very low."[1] The 126-h storm location in both the GFS and ECMWF deterministic forecasts are located near the far eastern edges of the ensemble envelopes, and the majority of members in both ensembles make landfall or are approaching the U.S. East Coast (Figs. 2a,b). The APSU forecast position at 126 h is also located to the east of the center of the ensemble envelope, but the ensemble is more evenly split, with nearly half of the members tracking Joaquin toward the U.S. East Coast and the rest away from the United States (Fig. 2c). It is worth pointing out that, unlike the APSU forecast, which is run at the same resolution and using the same physics as the ensemble forecasts, the ECMWF and GFS deterministic forecasts are run at higher resolution than their accompanying ensemble forecasts and also with slightly different tuned physics.

In addition to correctly forecasting that Joaquin would head eastward, the APSU forecast also sufficiently reproduces the best-track intensity and rapidly intensifies Joaquin into a major hurricane, although there is a difference in the exact timing of rapid intensification (RI) onset (Fig. 3). While the APSU deterministic forecast well captures the intensification of Joaquin, the PSU WRF EnKF ensemble contains very large intensity spread, with many members intensifying Joaquin into a major hurricane, while other members fail to forecast any intensification.

The large spread in track and intensity forecasts seen in the PSU WRF EnKF system will be examined further to determine and explain regions of IC errors that contributed to the forecast spread.

b. Joaquin's track and intensity spread

To reduce computational cost, 84-h forecasts are run with IC differences in specific regions (within 300 km and outside 600 km of the initial vortex center) removed; 84-h forecasts are sufficient to capture the period of track and intensity forecast divergence (Figs. 4a–c). The initial-position spread in the original real-time (CNTL) ensemble is ~60 km and increases to nearly 500 km by 84 h (Fig. 5a). The initial intensity spread of CNTL is ~5 hPa or ~10 kt and increases to ~35 hPa or ~30 kt by 84 h into the forecast and appears to asymptotically approach these values (Figs. 5b,c). It is also worth noting that the intensity spread appears saturated in the CNTL ensemble by ~60 h.

The effects of the perturbations to the environment are first isolated by relaxing the ICs of each member to the same APSU values within 300 km. The gradual relaxation to the APSU inner-core region is done over a distance of 300 km and uses a linear combination where a weight between 0 and 1 is assigned for APSU and the ensemble member. Inside of 300 km from the vortex center, the weight given to APSU is 1, and the weight given to the ensemble member is 0. As the distance increases beyond 300 km, the weight given to APSU linearly decreases, and the weight given to the ensemble member linearly increases until at a distance greater than or equal to 600 km from the initial storm

[1] Forecast discussion written at 1500 UTC 29 September 2015 by Pasch and Burke (available at http://www.nhc.noaa.gov/archive/2015/al11/al112015.discus.007.shtml?).

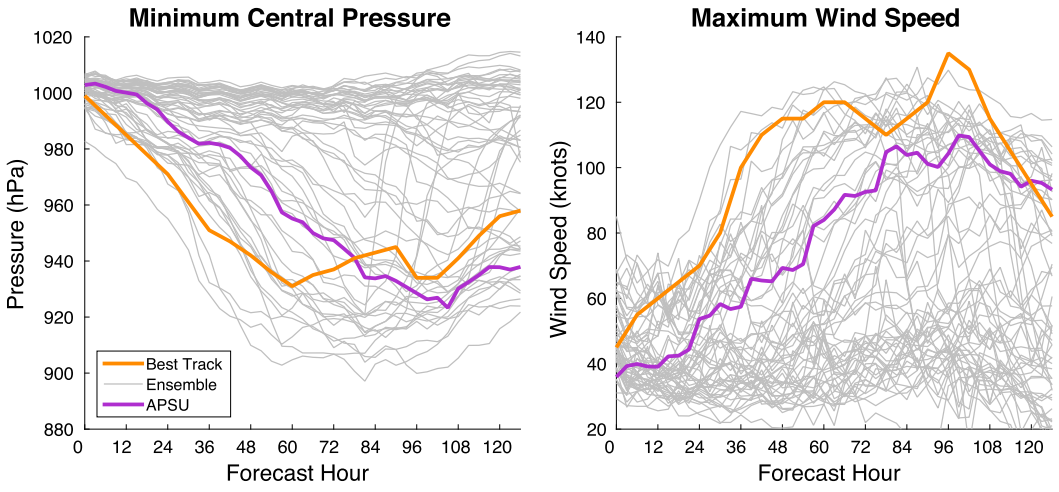

FIG. 3. Real-time ensemble and deterministic 126-h intensity forecasts from the PSU WRF EnKF system from 1200 UTC 29 Sep. Best-track intensity during this period is also shown.

center location, where the weight given to APSU is 0 and the weight given to the ensemble member is 1. The result of this approach is that each ensemble member now has identical ICs in the storm's inner-core region and only different ICs in the environment.

From the relaxed-to-APSU-inner-core ensemble ICs (Rcore), an additional 84-h forecast (Figs. 4d–f) is produced, and the forecast intensity and track spread can be compared with the CNTL ensemble (Figs. 4a–c). From the Rcore forecasts, we can see that a divergence in the track still occurs (Fig. 4d). Additionally, despite having no initial position spread in Rcore, this ensemble is the only one whose track spread approaches that of CNTL (Fig. 5a). The 84-h position spread of Rcore is ~80% of that of CNTL. The difference between the final position spread of CNTL and Rcore is nearly identical to the difference in the position spread at 0 h for those experiments, suggesting that initial position spread may contribute the remaining 20% in 84-h position spread between CNTL and Rcore. These results suggest that Joaquin's large track forecast spread likely occurs regardless of perturbations to the initial storm's inner-core region. This agrees with many previous studies that have shown that the inner-core region is not a major source of uncertainty in determining TC motion (George and Gray 1976; Fiorino and Elsberry 1989; Cheung and Chan 1999b; Chan and Li 2005).

While the track divergence is still clearly seen when the initial storm's inner-core perturbations are removed, the intensity spread is greatly reduced compared to CNTL. There are essentially no differences in the intensity between the Rcore ensemble members over the first 12 h, as the spread in terms of minimum central pressure is less than 2 hPa and maximum wind speed is less than 3 kt (Figs. 5b,c). Differences in intensity among the ensemble members begin to develop beyond 12 h, as the storm positions begin to diverge, and we speculate that differences in the synoptic environment, such as vertical wind shear and relative humidity variability, begin to have an effect. By 84 h, the minimum central pressure spread has grown to approximately 28 hPa, and the maximum wind speed spread is near 25 kt. While the intensity spread has increased substantially, the intensity spread is only ~80% of CNTL. This result suggests that the IC differences in the environment have a significant effect on the intensity forecast of Joaquin but do not account for the full range of the intensity forecast spread within the first 84 h, consistent with Emanuel and Zhang (2016), who found that initial intensity errors dominate within the first 48 h but environmental IC difference errors dominate thereafter. While the ensemble intensity spread of Rcore is less than CNTL, the rate of intensity error growth after ~12 h is nearly identical, suggesting that the rate of intensification is similar and the uncertainty results from whether or not intensification occurs. Unlike CNTL, the intensity spread is still increasing in the Rcore ensemble experiment at 84 h.

We next isolate the effects of the perturbations to the storm's inner-core region by relaxing each ensemble member to the same environment, chosen here to be from the deterministic GFS. Unlike the real-time system, however, the background error covariance perturbations (Barker et al. 2004) to the environment are not applied. Inside of 300 km from the vortex center, the weight given to GFS is 0, and the weight given to the ensemble member is 1. As the distance increases beyond 300 km, the weight given to GFS linearly increases, and

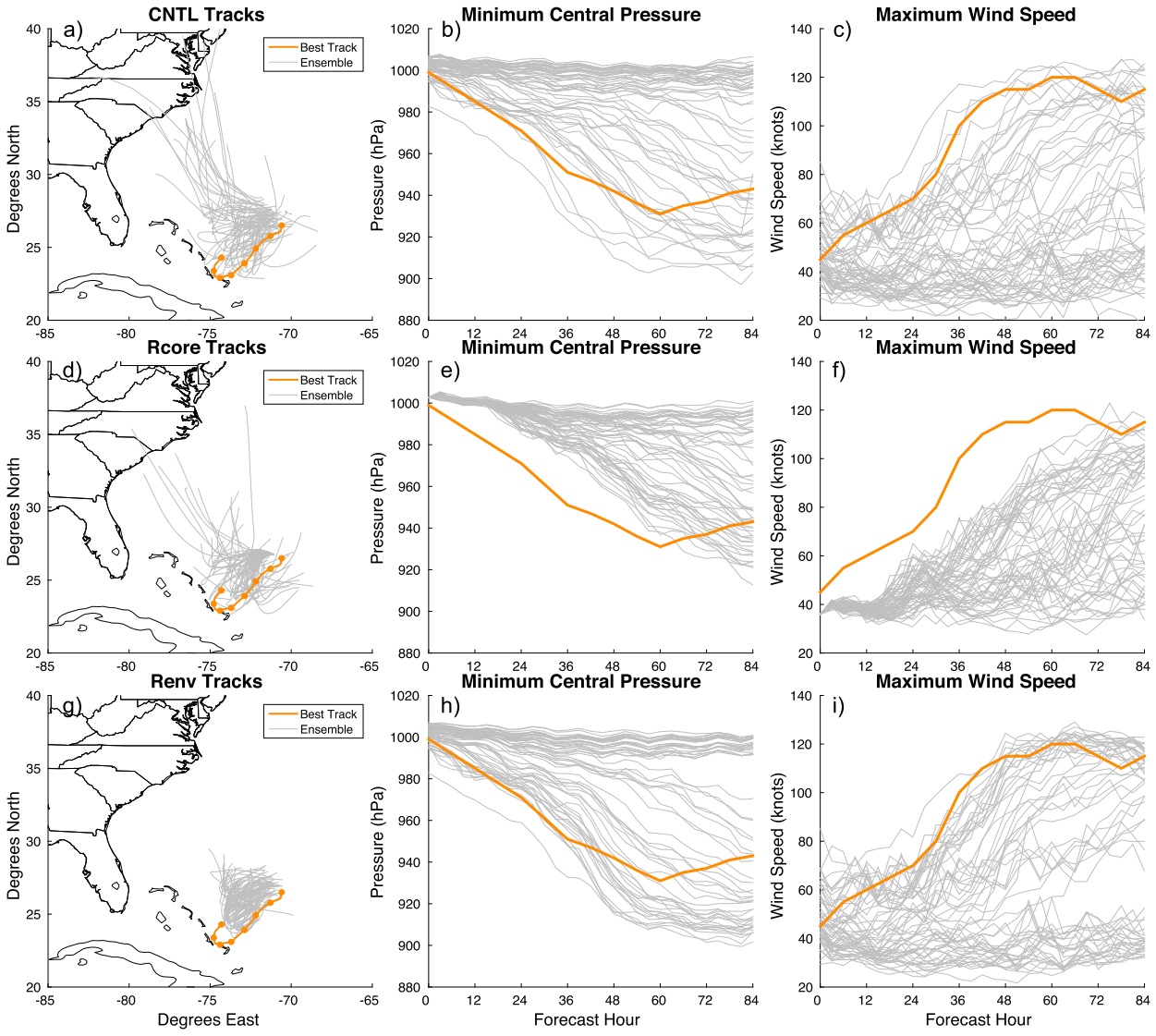

FIG. 4. The 84-h ensemble forecasts of (a) track, (b) minimum central pressure, and (c) maximum wind speed from real-time (CNTL) ensemble; (d) track, (e) minimum central pressure, and (f) maximum wind speed for Rcore ensemble; and (g) track, (h) minimum central pressure, and (i) maximum wind speed for Renv ensemble. Best-track intensity and track during this period are also shown. Markers on best-track forecast denotes location every 12 h.

the weight given to the ensemble member linearly decreases until at a distance greater than or equal to 600 km from the initial storm center location, where the weight given to GFS is 1 and the weight given to the ensemble member is 0. The result of this approach is that each ensemble member now has identical ICs in the environment and the ICs are different only within the storm's inner-core region.

Using the relaxed-to-GFS-environment ICs (Renv), an 84-h ensemble forecast is simulated (Figs. 4g–i), and the resulting forecast intensity and track spread are compared with the original CNTL ensemble. The Renv members do not produce a track divergence similar to CNTL or Rcore (Figs. 4a,d,g). Despite having the same initial position spread as CNTL (~60 km), the 84-h position spread is less than 150 km, less than 30% of CNTL (Fig. 5a). This result suggests that IC differences in the environment are necessary for the track divergence seen in the real-time ensemble and further confirms that IC differences in the storm's inner-core region alone do not play a significant role in the track divergence.

While the IC differences in the storm's inner-core region do not significantly impact the track of Joaquin, minimum central pressure spread doubles (from 5 to 10 hPa) in the first ~24 h, and maximum wind speed spread doubles (from 11 to 22 kt) in the first ~30 h

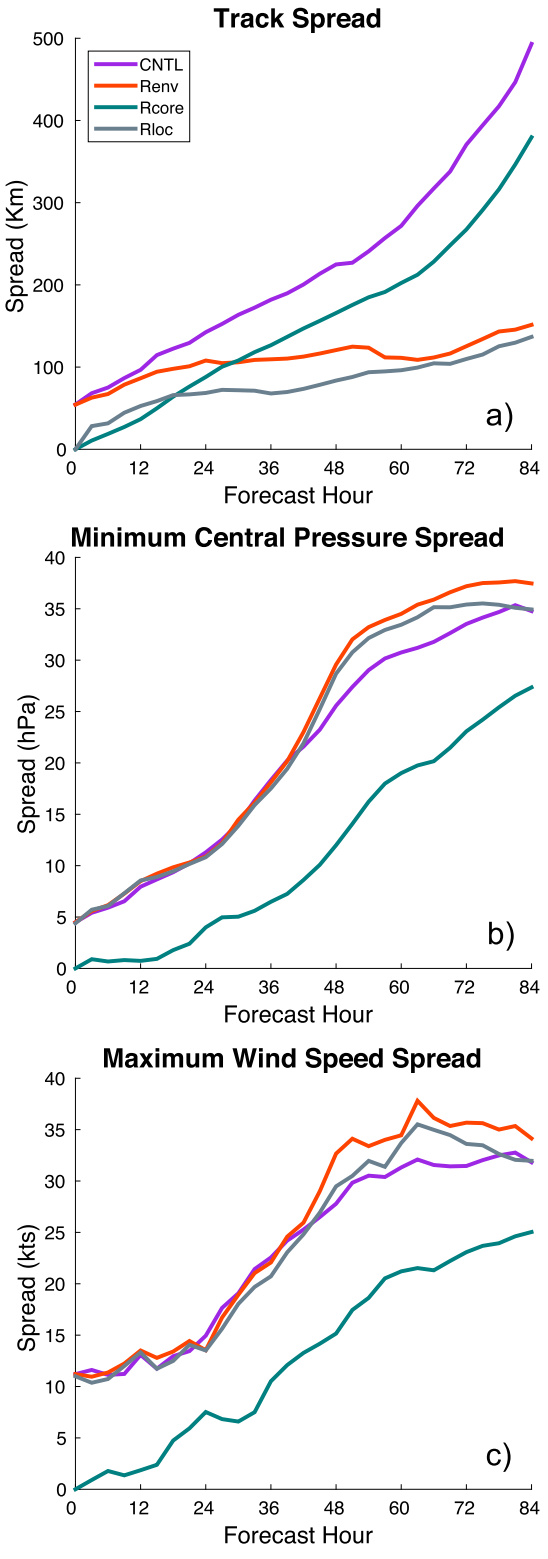

FIG. 5. Ensemble (a) track, (b) minimum central pressure, and (c) maximum wind speed spread comparison of CNTL, Renv, Rcore, and Rloc ensembles.

(Figs. 5b,c). The intensity spread of Renv almost exactly matches the spread of CNTL, demonstrating that IC differences to the storm's inner-core region alone were able to replicate the intensity spread of the CNTL ensemble. Similar to CNTL, the intensity spread appears saturated in the Renv ensemble experiment near 60 h. The IC differences to the storm's inner-core region are clearly and expectedly important in the resulting intensity spread. The proximity of the initialization time to the RI-onset time of Joaquin likely enhanced the importance of inner-core IC differences as in Emanuel and Zhang (2016), in which it was demonstrated that initial intensity errors were the dominant source of error for TCs that are approaching RI.

Last, initial position differences were also removed from the Renv ensemble by relocating the initial vortex to the location of APSU (which is less than 100 km from the best-track position). The 84-h ensemble forecasts from this ensemble, referred to hereafter as Rloc, were nearly identical to Renv (not shown). The similarity between Renv and Rloc ensemble forecasts demonstrates that initial position spread is not a major source of uncertainty resulting in larger intensity forecast uncertainty (Figs. 5b,c).

In summary, a comparison of track forecast spread from the CNTL, Rcore, Renv, and Rloc reveals that the region 300 km or greater from the storm center (i.e., the storm environment) contains the dominant source of IC differences that contribute to the track spread of Joaquin (Fig. 5a). We also compared the intensity forecast spread in terms of both minimum central pressure and maximum wind speed, and IC differences in the region within 300 km from the storm center (storm's inner-core region) are the dominant source of initial condition differences that contribute to the intensity spread (Figs. 5b,c).

Quantitative analysis of a real-time convective-permitting ensemble forecast demonstrates that, while IC differences in the environment can result in appreciable intensity spread, the intensity spread of the real-time Joaquin ensemble forecast is shown to be replicated by IC differences to the storm's inner core alone. Furthermore, these results demonstrate that if short-term intensity forecast spread is to be reduced for Joaquin at this initialization time, then IC errors to the inner-core region must be reduced. This is because the intensity spread in this case appears to saturate more quickly and to the same value as a result of IC errors to the storm's inner core. Conversely, while the initial position uncertainty had a nonnegligible contribution, the track spread predominantly resulted from IC differences to the environment. The factors within each of these regions that led to large track and intensity spread will now be examined more closely.

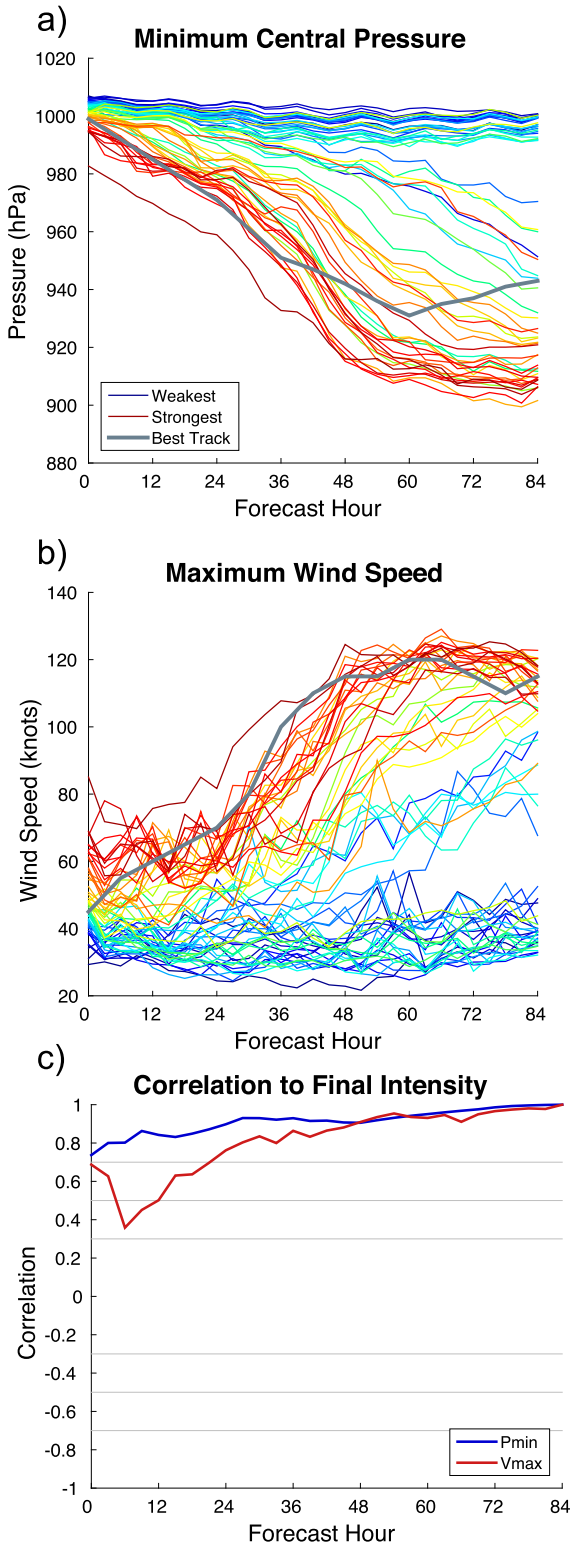

FIG. 6. (a),(b) Ensemble intensity forecasts from Rloc ensemble colored by initial strength (strongest = dark red; weakest = dark blue) and best-track intensity and (c) correlation of intensity throughout forecast to 84-h intensity.

c. *Explaining Joaquin's intensity spread*

Because the intensity forecast spread was shown to be more sensitive to the storm's inner-core IC differences than environmental or initial vortex position differences, we examined the intensity forecasts from the Rloc ensemble to identify the leading factors that led to the large intensity spread. The Rloc ensemble forecast, when colored by initial storm intensity, demonstrates a very strong sensitivity to final (84 h) storm intensity (Figs. 6a,b). The ensemble members with the strongest initial vortices generally intensified most significantly, and the initially weaker members remained relatively weak throughout the forecast period. This strong sensitivity of forecast intensity to initial intensity agrees with that found by others (e.g., Emanuel and Zhang 2016; Munsell et al. 2013; Sippel and Zhang 2010; Sippel et al. 2011) who discussed that initial intensity uncertainty can significantly impact the forecast intensity uncertainty, particularly for TCs about to undergo RI. This is especially true when the intensity of storms is weaker as opposed to stronger (e.g., Emanuel and Zhang 2016; Munsell et al. 2013; Sippel and Zhang 2010; Sippel et al. 2011). Consistent with these results, the members in this ensemble whose initial intensities are stronger than the best track all intensify, while only some of the members that started out weaker than best track intensify. Finally, Fig. 6c shows the time-lag correlation between minimum pressure (Pmin) or maximum wind speed (Vmax) throughout the forecast and their final values. This result suggests that, in this case, the initial intensity is a good predictor of the forecast intensity.

To better understand why the initial intensity is such a strong determining factor in the final intensity, composite east–west cross sections through the storm center are created to examine the vertical structure of the stronger (Strong Initial) and weaker (Weak Initial) (as compare to best-track intensity) ensemble members. At 0 h, Strong Initial has a more symmetric wind field and a stronger and deeper absolute vorticity column than Weak Initial (Fig. 7). In addition, at 0 h, Strong Initial has higher values of RH closer to the surface center and over a deeper layer on the downtilt (eastern) side than Weak Initial (Fig. 8). Interestingly, however, Weak Initial actually has a slightly stronger midlevel warm core than Strong Initial. The temperature perturbation is calculated as the difference from the environmental temperature, defined as the mean temperature at each vertical level between 600 and 800 km from the TC center for each member. By 12 h, the depth of the vortex of Strong Initial has increased substantially and now extends above 200 hPa (Fig. 7). Conversely, the depth of

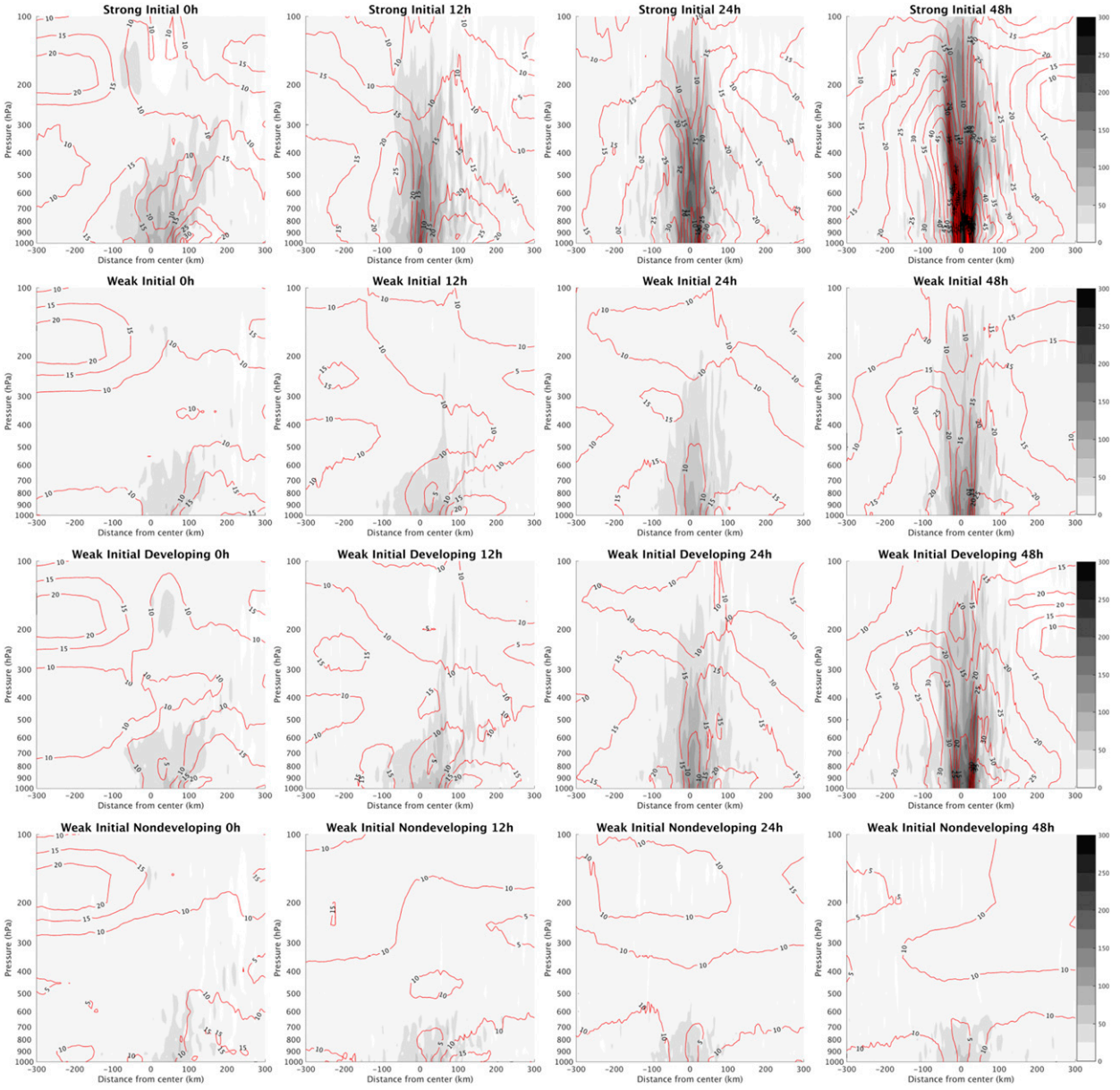

FIG. 7. Composite east–west vertical cross sections through the vortex center from the Rloc ensemble of absolute vorticity (shaded) and total wind speed (contoured every 5 m s^{-1}). (top row) Members of the ensemble whose initial Pmin is less than that of best track. (second row) Members of the ensemble whose initial Pmin is greater than best track. (third row) Members whose initial Pmin is greater than best track and intensify. (bottom row) Members whose initial Pmin is greater than best track and do not intensify.

the vortex of Weak Initial is relatively unchanged, although some minor strengthening is seen. Furthermore, by 12 h, Strong Initial has higher RH now on both sides of center than Weak Initial (Fig. 8). Strong Initial also now has developed an upper-level warm core, unlike Weak Initial. Strong Initial continues to intensify between 24 and 48 h as the depth of the vortex increases further and the absolute vorticity throughout the troposphere increases along with the wind speed and the warm core (Figs. 7 and 8). Weak Initial also appears to begin to intensify during this time but is still considerably weaker by 48 h.

It is worth noting that the process leading up to and through the intensification between the two groups is similar but appears to take longer for Weak Initial than Strong Initial (Figs. 7 and 8). The wind field first appears to become more symmetric, the vortex appears to deepen, and higher RH air moves closer to the storm center and

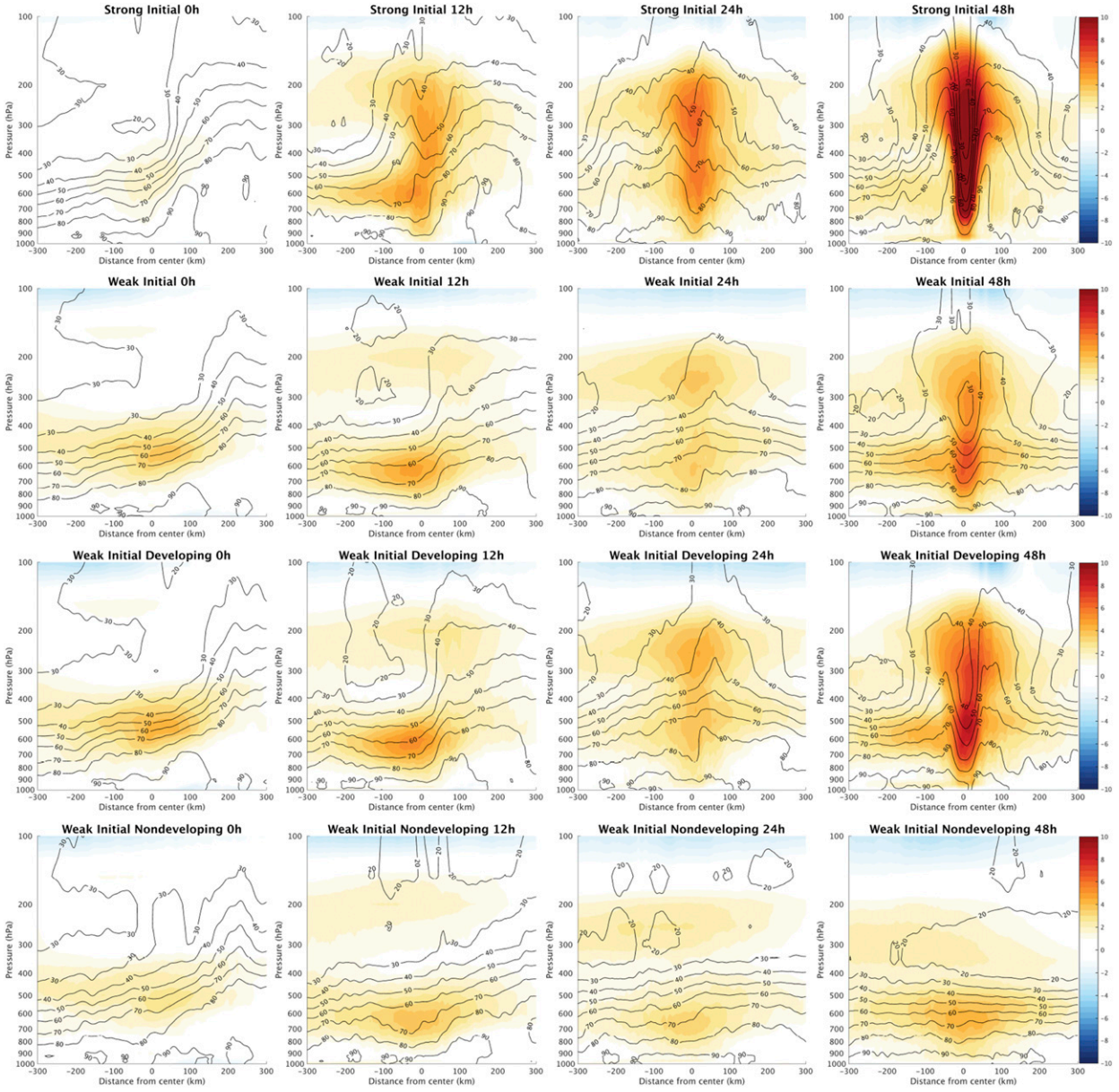

FIG. 8. As in Fig. 7, but for temperature perturbation (shaded) and relative humidity (contoured every 10%).

then wraps around to both sides. At this time (~12 h in Strong Initial and ~24 h in Weak Initial), the entire vortex begins to intensify, the maximum wind speed increases, and an upper-level warm core develops.

To understand the cause of the larger intensity forecast uncertainty for members initially weaker than best-track intensity, developing (Weak Initial Developing) and nondeveloping (Weak Initial Nondeveloping) members are separated and composite east–west cross sections through the storm center compared. At 0 h, Weak Initial Developing appears marginally stronger than Weak Initial Nondeveloping and has higher absolute vorticity and wind speeds (Fig. 7). Additionally, the midlevel warm core is stronger at 0 h in Weak Iinitial Developing and the RH is considerably higher on the downtilt (east) side, especially above 500 hPa (Fig. 8). By 12 h, Weak Initial Developing has a more symmetric wind field, unlike Weak Initial Nondeveloping (Fig. 7). Also by 12 h, the upper-level relative humidity (RH) has increased substantially in Weak Initial Developing on the downtilt side and reduced in Weak Initial Nondeveloping (Fig. 8). By 24 h, the absolute vorticity and wind speeds have begun to increase in Weak Initial Developing, and an upper-level warm core has developed (Figs. 7 and 8). This

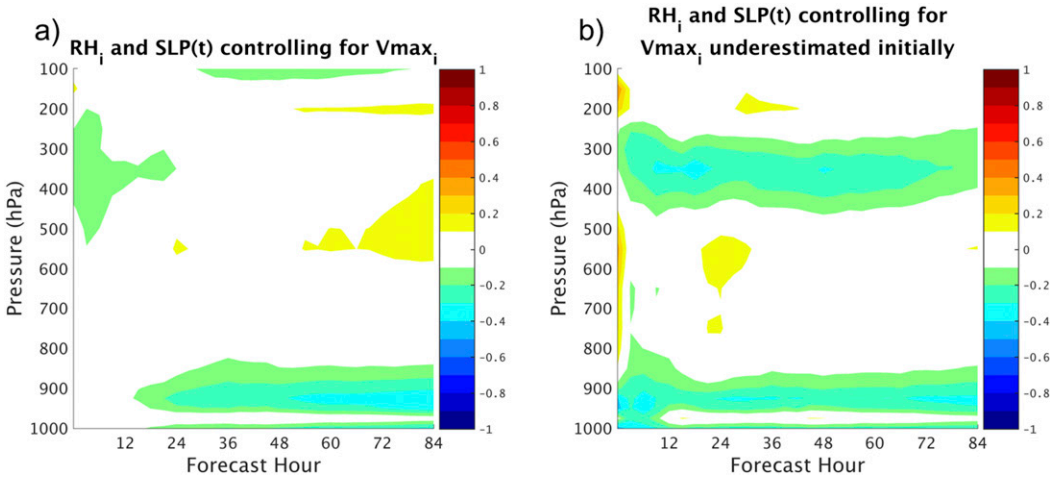

FIG. 9. Semipartial correlation of initial relative humidity (averaged within 300 km of storm center) to minimum pressure through time, controlling for initial maximum wind speed for (a) all ensemble members and (b) only ensemble members whose initial minimum central pressure was greater than the best-track estimate (31 members).

intensification continues through 48 h. No intensification is seen by 48 h in Weak Initial Nondeveloping, and no signs of upcoming intensification are visible either.

To more quantitatively examine secondary factors of initial condition differences that may have affected the intensity forecasts of Hurricane Joaquin, specifically the inner-core moisture differences in members whose intensities were initially weaker than best-track intensity, we can examine the semipartial correlation between Pmin and initial mean RH within 300 km of the vortex center while controlling for initial Vmax. To do so, we used the approach of Sippel and Zhang (2010) and Sippel et al. (2011), which used the following semipartial, or part, correlation equation:

$$r_z(x,y) = \frac{r(x,y) - r(x,z)r(y,z)}{\sqrt{1 - r^2(y,z)}}, \qquad (1)$$

where x is RH at time $t = 0$, y is the Pmin at time t, and z is Vmax at time $t = 0$.

By ~24 h (approximately the time of RI onset), a weak semipartial correlation is seen between the initial low-level RH (950–800 hPa) and Pmin (Fig. 9a). This weak correlation remains visible throughout the remainder of the forecast. The negative partial correlation between low-level RH and Pmin implies that ensemble members with higher initial mean low-level RH correspond with stronger final storms. Because all of the ensemble members whose initial intensities are stronger than best track ($\text{Pmin}_i <$ best track) intensify, the subgroup of only ensemble members whose intensities are initially weaker ($\text{Pmin}_i >$ best track) is also examined (Fig. 9b). Again, a weak negative semipartial correlation is seen between the initial low-level RH (950–800 hPa) and Pmin. In addition, a weak negative correlation is also seen between initial upper-level RH (400–300 hPa) and Pmin. Because we are examining the effects of IC differences in inner-core moisture, we cannot determine what caused these differences in ICs as they are already present at the initial time. However, we can evaluate how these initial moisture differences impact the subsequent forecast intensity of Joaquin. We speculate that ensemble members that have higher RH near the surface allow for the development of stronger convection, because the low levels are already closer to saturation. This stronger convection then has a positive feedback on storm intensity. The stronger convection allows for more efficient latent heat release and stronger surface winds, which then result in a larger energy transfer between the ocean and the atmospheric boundary layer. A more detailed analysis of the impact of low-level moisture in this ensemble is found in Emanuel and Zhang (2017). Furthermore, the higher RH in the 300–400-hPa region may be important to reduce the effects of dry-air entrainment and allow for more efficient latent heat release and a stronger upper-level warm core, as seen in Fig. 8. Examination of partial correlations between other quantities and final Pmin yielded no significant correlations (not shown).

Overall, the results found here are in good agreement with Torn and Cook (2013), who found that pregenesis systems that are initially stronger tend to remain stronger and are associated with higher moisture throughout the column. It appears based on the results found here that this can be extended to a tropical storm prior to intensification. Additionally, previous studies have found preconditioning by convection prior to RI onset (Chen and Gopalakrishan 2015); that appears in the Joaquin ensemble, and

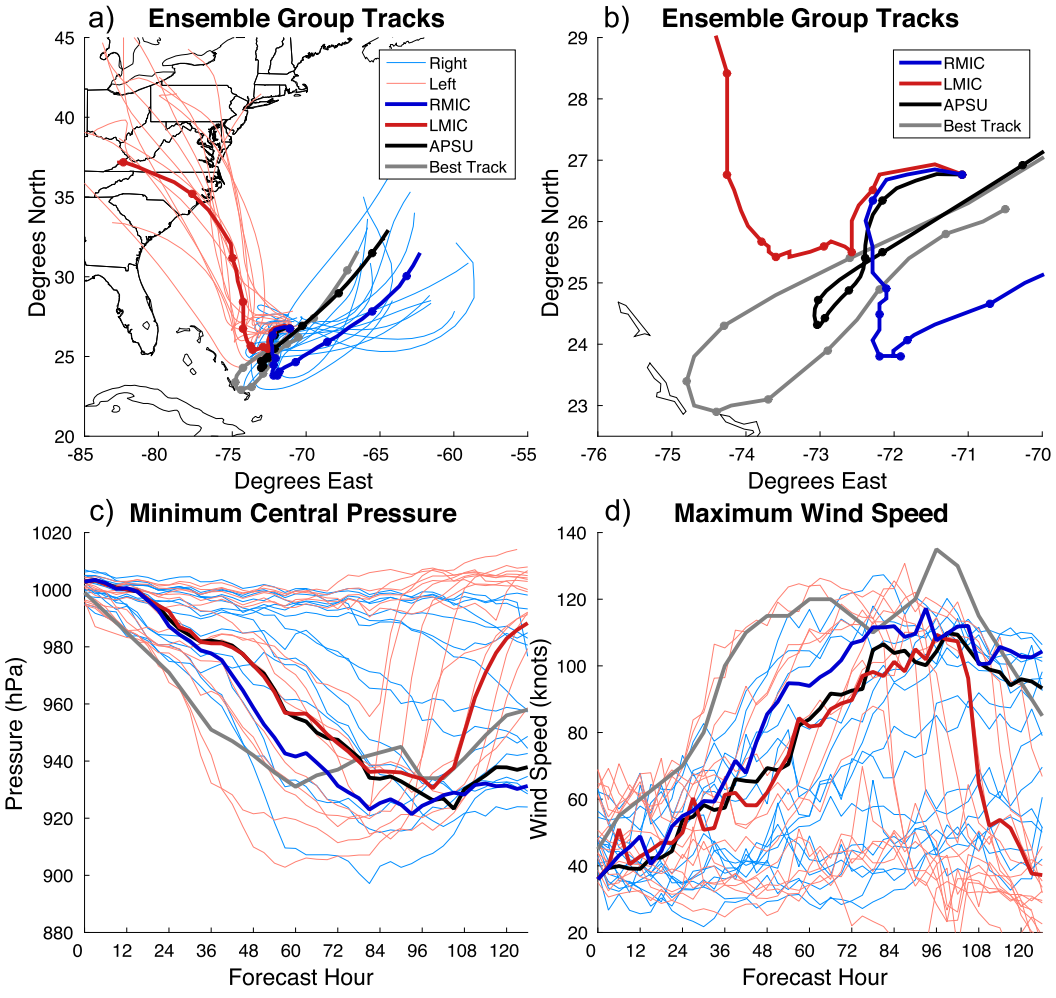

FIG. 10. The 126-h forecasts of (a),(b) track, (c) minimum central pressure, and (d) maximum wind speed for composite group members and mean initial condition experiments.

upper-level RH appears to increase near the center prior to intensification. This is also consistent with Tang and Emanuel (2010), who demonstrated that midlevel ventilation of dry air reduces the maximum intensity of a TC. In addition, the storm appears to become more symmetric prior to RI onset, consistent with Zhang and Tao (2013) and Tao and Zhang (2014, 2015). Furthermore, the formation of an upper-level warm core is apparent in the Joaquin ensemble, similar to Chen and Zhang (2013), although it appears to develop after intensification has begun. While the impact of initial moisture differences within 300 km may appear small here, Emanuel and Zhang (2017) have shown more systematically that weaker storms are more sensitive to initial moisture differences than stronger storms and that IC differences in water vapor mixing ratio alone are enough to result in appreciable intensity forecast uncertainty for Hurricane Joaquin, using the same ensemble shown here.

d. Composite track groups

To examine the cause of the track bifurcation between the ensemble members that track toward the U.S. East Coast and those that track away from the coast, we separated the real-time ensemble into two composite groups: the Left group—whose members incorrectly forecasted Joaquin to track toward the coast and make landfall—and the Right group—whose members correctly forecasted Joaquin to track eastward. Each group contains 15 ensemble members, and their track and intensity forecasts are shown in Fig. 10. There is no apparent intensity dependence on the forecast track of Joaquin as both the Left and Right composite groups contain initially weak and strong ensemble members and have members of variable intensity throughout the simulation, except near the end of the forecast period, where the Left composite group members have all made

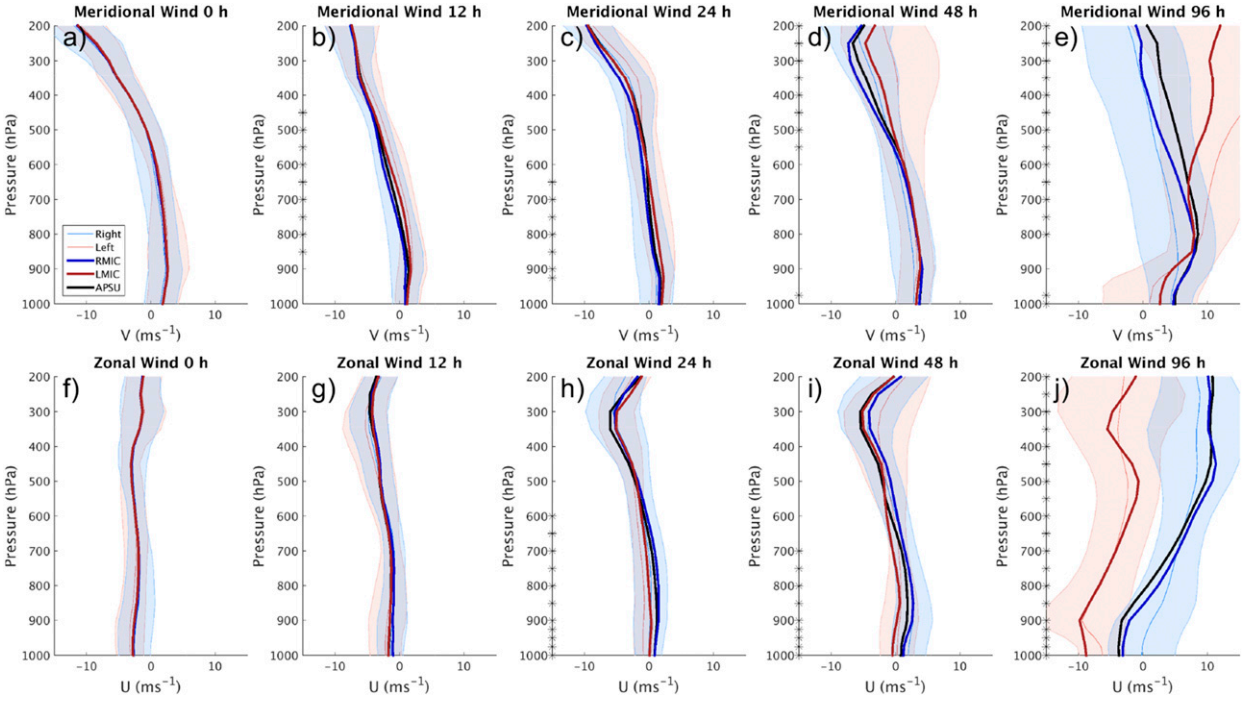

FIG. 11. Vertical profiles of zonal and meridional steering winds of Left and Right composite groups. Shaded regions represent two standard deviations of composite track groups, thin lines represent mean of composite members, and thick lines represent composite group mean initial condition forecasts. Asterisks on *y* axis denote levels where Left and Right groups are statistically different at the 95% confidence interval.

landfall and weakened. This is consistent with the track spread being insensitive to the removal of perturbations within 300 km of the initial vortex center.

In addition to the forecasts of the two composite group ensemble members, Fig. 10 also shows (thick lines) the forecasts that result from ICs generated by compositing the ICs of the members of the two groups, with each storm's inner-core region relaxed to APSU within 300 km. Both the Left mean-IC (LMIC) and Right mean-IC (RMIC) track forecasts are comparable to that of the ensemble members within each respective composite group and are near the center of the respective composite group ensemble track envelope. The track bifurcation between the LMIC and RMIC runs first appears between 12 and 24 h and is visible in a north–south position difference, with the RMIC position located farther to the south than LMIC (Fig. 10b). At ~24 h, an east–west position difference becomes visible, with the LMIC position located farther west than RMIC. In addition, the intensity forecasts of the LMIC and RMIC are very similar until the LMIC forecast makes landfall. It should be noted that the forecast track of APSU is within the Right group, and therefore a comparison between the LMIC and APSU forecasts is appropriate to examine causes of the track bifurcation.

To highlight the underlying cause of track bifurcation, Fig. 11 displays the area-mean vertical profiles of the zonal and meridional winds from the optimal steering flow (Galarneau and Davis 2013) used to diagnose the steering flow in the vicinity of the TC. However, in order to compare differences across the ensemble, the optimal steering was chosen to be invariant for all ensemble members. The removal radii and depth that had the lowest mean errors when compared to the actual motion over the first 48 h is used for the remainder of this study. This corresponded to a TC removal radii of 4° and a vertical depth of 850–350 hPa and had a mean error of ~1 m s^{-1} (not shown), similar to that found in Galarneau and Davis (2013). While there is initially no clear distinction between the meridional or zonal winds in the steering region (Figs. 11a,f), differences between the Left and Right composite groups begin to appear between 12 and 24 h (Figs. 11b,c,g,h). Between 12 and 24 h, the meridional steering flow for the Right group generally has a more negative meridional component than the Left group, especially in the low and midlevels between 850 and 450 hPa (Figs. 11b,c). By 24 h, we can also begin to see differences between the Left and Right composite groups in the zonal steering flow, especially in the low levels between 850 and 600 hPa (Fig. 11h). Left members are generally embedded in near-zero or slightly

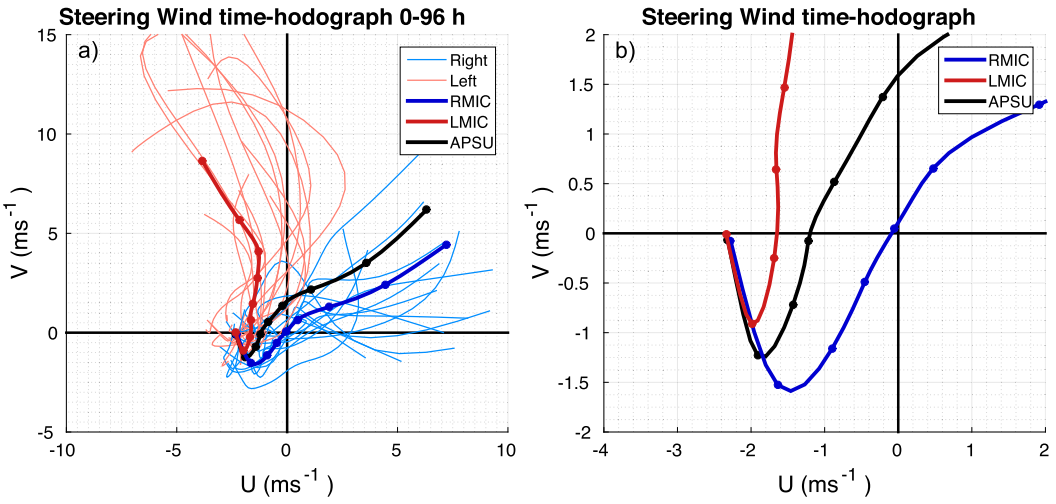

FIG. 12. Time hodograph of optimal mean steering flow for (a) composite groups and (b) zoomed in to more clearly illustrate differences leading up to the time of track divergence. Markers on APSU, LMIC, and RMIC denote every 12 h.

easterly flow, while Right members appear to be embedded in near-zero or slightly westerly flow. Beyond 24 h, the Right composite group members generally have a stronger positive *U* component. The zonal steering-flow differences at 24 h are maximized in the low levels but subsequently extend throughout the entire troposphere by 96 h (Fig. 11j). This stronger positive *U* component of the steering flow in the Right composite group is as expected since these members track farther east.

The differences in steering flow between the Left and Right composite groups are further highlighted by the time hodograph of the optimal steering flow (Fig. 12). The Right composite group ensemble members generally have a more negative meridional component to their steering flow over the first 48 h, which results in a more southern position by 48 h (Figs. 10a,b). In addition, between 48 and 96 h, the Right composite ensemble members, unlike the Left composite group members, generally have a positive *U* component to their steering flow, causing the Right composite group to track away from the U.S. East Coast after 48 h.

Because the steering flow appears to be quite important in explaining the track bifurcation of Joaquin, we analyzed the time-lag ensemble correlations between optimal steering area-mean meridional and zonal wind profiles and the longitude of the storm center at 96 h to determine vertical levels where steering-flow differences ultimately result in the tack bifurcation and when significant differences in the steering flow developed (Fig. 13). By ~12 h, a correlation of −0.5 exists between the meridional steering flow between 800 and 500 hPa and the longitude of the storm center at 96 h (Fig. 13a). This result suggests that ensemble members with a weaker positive, or even negative, *V* component would expectedly have a more southern location of the storm center and, in time, would correspond with a storm center location that is farther to the east at 96 h. Beyond ~48 h, the Left ensemble members are accelerating north more quickly than the Right members as a result of meridional wind differences throughout the troposphere. In addition, by ~24 h, a correlation of at least 0.5 exists between the low- and midlevel zonal steering wind and the longitude of the storm center at 96 h (Fig. 13b). This correlation is confined more to the low levels until ~60 h, when it eventually begins to extend throughout the entire troposphere. The importance of mid- to low-level steering winds has been noted previously by Wu and Emanuel (1995) for Hurricane Andrew.

Important differences in the steering flow appear initially in the low- and midtropospheric steering winds (around 700 hPa). Using the intensity-specific steering as defined by Velden and Leslie (1991) and Velden (1993), these differences are found in a region that would affect the steering of storms of all intensities and therefore may explain why intensity does not appear to strongly influence the track bifurcations in this ensemble forecast. To further demonstrate this quantitatively, Fig. 14a displays the ensemble correlation between Pmin and the storm center longitude at 96 h. If a relationship existed between forecast intensity and track, we would expect a significant correlation; however, this correlation remains insignificant through 96 h. Also shown in Fig. 14a, insignificant correlation between initial storm center longitude–latitude and 96-h storm center longitude

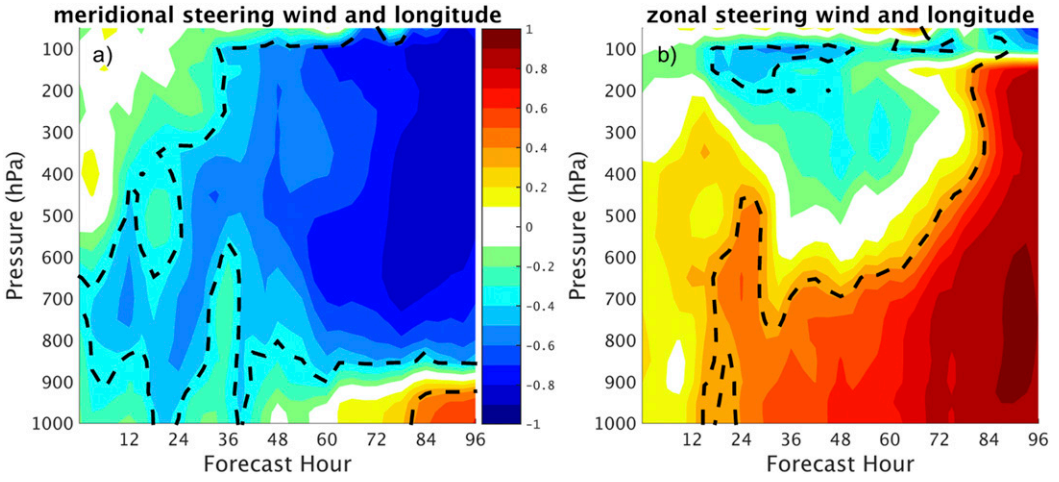

FIG. 13. Correlation between (a) meridional steering wind and storm center longitude at 96 h and (b) zonal steering wind and storm center longitude at 96 h from optimal mean steering flow. Dashed lines highlight regions where correlations are statistically significant at the 95% confidence interval.

further demonstrates that the initial position differences were not a dominating factor resulting in the track bifurcation. A weak correlation between the 24-h storm center latitude and the 96-h longitude suggests that storms located farther south are more likely to be located farther east at 96 h. This correlation remains negative and increases as forecast time increases. Furthermore, a strong correlation between 48-h storm center longitude and 96-h longitude suggests that the east–west track bifurcation has already occurred.

To attempt to highlight the region in the ICs that ultimately resulted in the track bifurcation, the correlations of initial 700-hPa fields and the storm center longitude at 96 h were examined. The 700-hPa level was chosen because correlations between steering winds and storm center longitude at 96 h highlighted this layer (Fig. 13). Correlations between the 700-hPa geopotential height and the storm center longitude suggest higher geopotential heights to the west and near the initial storm center location may be associated with a location farther east at 96 h (Fig. 14b). Also visible in the correlations between the 700-hPa geopotential height and the 96-h storm center longitude is a negative correlation to the east of the initial storm location, which suggests that lower geopotential heights to the east of the storm may be associated with a storm location farther to the east at 96 h. Consistent with the signal seen in the 700-hPa geopotential height correlation and ~600–900 km to the west of the initial storm location, a positive correlation between the initial 700-hPa meridional wind and the storm location at 96 h suggests that stronger southerly winds in this region may be associated with a storm location farther east at 96 h (Fig. 14c). A weak negative correlation between the 700-hPa meridional wind and the 96-h storm center longitude to the north of the initial storm location suggests that a more negative meridional component in this region may be associated with a storm center position farther east at 96 h.

Large-scale differences that may have influenced the steering flow and the subsequent track of Hurricane Joaquin are further identified by comparing the APSU forecast with the LMIC forecast in Fig. 15. The only differences in the ICs of these simulations are found at distances greater than 300 km from the initial storm center, isolating the effects of the environmental IC differences that cause most of the track spread. At 0 h, differences in the 700-hPa geopotential height are less than ~10 m, and the 700-hPa winds vary by less than ~5 kt (Figs. 15a–c). Consistent with the correlations in Fig. 14, APSU has higher initial 700-hPa geopotential heights to the northwest and southwest and lower geopotential heights to the east of the initial position between ~600 and 1200 km from the initial storm location than LMIC. Also consistent with the correlation to geopotential height, APSU has stronger 700-hPa meridional winds to the west of the initial storm center between 600 and 1200 km from the initial storm center. Over the first 24 h, APSU has slightly higher 700-hPa geopotential heights over the eastern United States and slightly lower 700-hPa geopotential heights over the Atlantic Ocean to the east of Joaquin (Figs. 15d–f). These two regions of geopotential height differences may be of some importance, since by 24 h, there are indications that Joaquin is located farther south in APSU than in the LMIC case, and therefore, the track

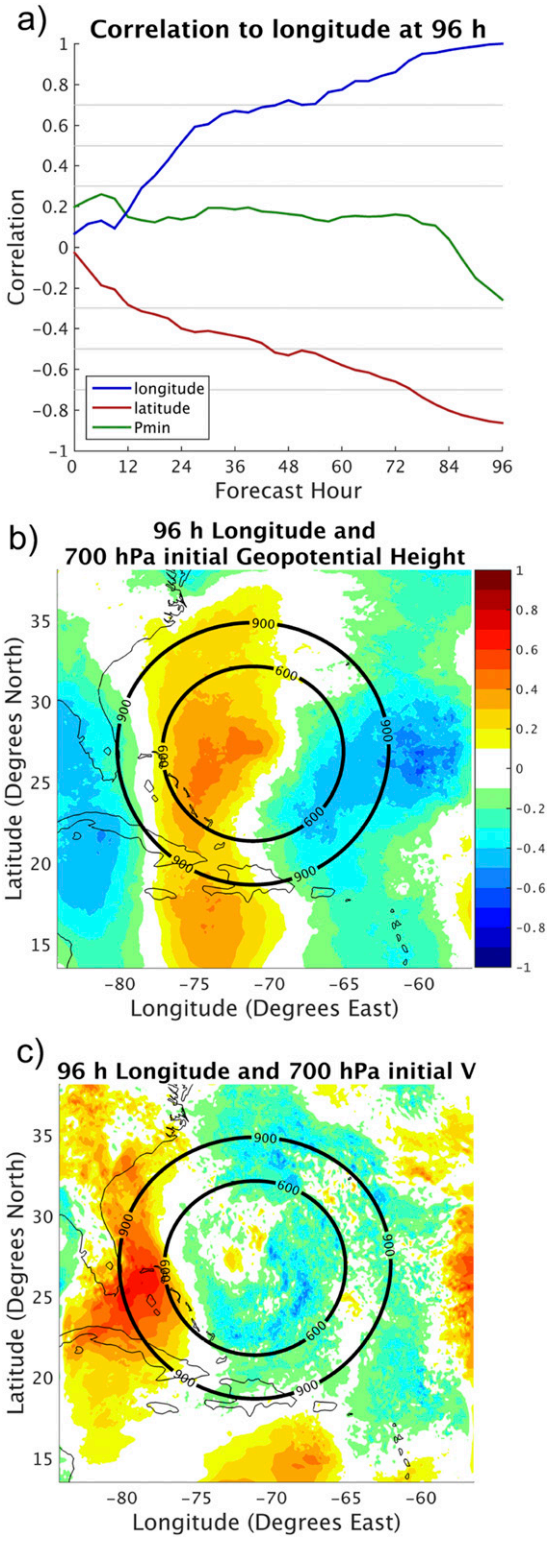

FIG. 14. Ensemble correlations of (a) storm center longitude, storm center latitude, and Pmin; (b) initial 700-hPa geopotential height; and (c) initial 700-hPa meridional wind component V with storm center longitude at 96 h.

divergence is already beginning to occur. There are also differences in the low pressure system located over the northeast Atlantic Ocean within the first 24 h (not shown); however, this system is located quite far from Joaquin and likely does not play a major role in the track of Joaquin, as will be shown later.

By 48 h, differences in the large-scale environments of APSU and LMIC are more clearly defined (Figs. 15g–i). At this time, the strengthening mid- to upper-level low pressure system over the southeastern United States is located slightly farther to the south in LMIC. In addition, a developing low-level system east of Joaquin is stronger in APSU than in LMIC. After 48 h, the mid- to upper-level low pressure region over the southeastern United States is consistently farther south in LMIC than in APSU (Figs. 15j–l). This north–south shift in the location of the mid- to upper-level low pressure region over the United States, coupled with the north–south shift in the position of Joaquin after 24 h, may be important in explaining the resulting track bifurcation of Joaquin. A more northern position of Joaquin at 24 h coupled with a more southern mid- to upper-level low pressure region over the southeastern United States by 48 h, similar to LMIC, is more likely to result in steering flow with a more negative zonal component, which will track Joaquin toward a landfall on the U.S. East Coast. On the other hand, a more southern position of Joaquin at 24 h coupled with a more northern mid- to upper-level low pressure region over the southeastern United States, as in APSU, is more likely to result in steering flow with a more positive zonal component that steers Joaquin to the east.

e. Diagnosis of contributing track bifurcation factors

Because no obvious IC differences in the large-scale synoptic features in the vicinity of Joaquin between the LMIC and APSU can be definitively linked to the track divergence, the dominant region of IC differences that results in the track divergence will be determined through a more rigorous approach. To do so, we will test the impact of gradually relaxing LMIC to the APSU *environment* beyond various radii and the impact of gradually relaxing LMIC to the APSU *inner-core region* within various radii.

We will first discuss the sensitivity to relaxing the environment of LMIC to the APSU environment beyond radii of 1200 (RE1200), 900 (RE900), 600 (RE600), and 300 km (RE300) from the initial storm center location, with blending done over a 300-km distance (e.g., 1200–1500, 900–1200, 600–900, and 300–600 km). This is done identically to the Renv experiment except the radius at which the relaxation begins is now varied. No IC differences between APSU and LMIC remain beyond 300 km outside these radii.

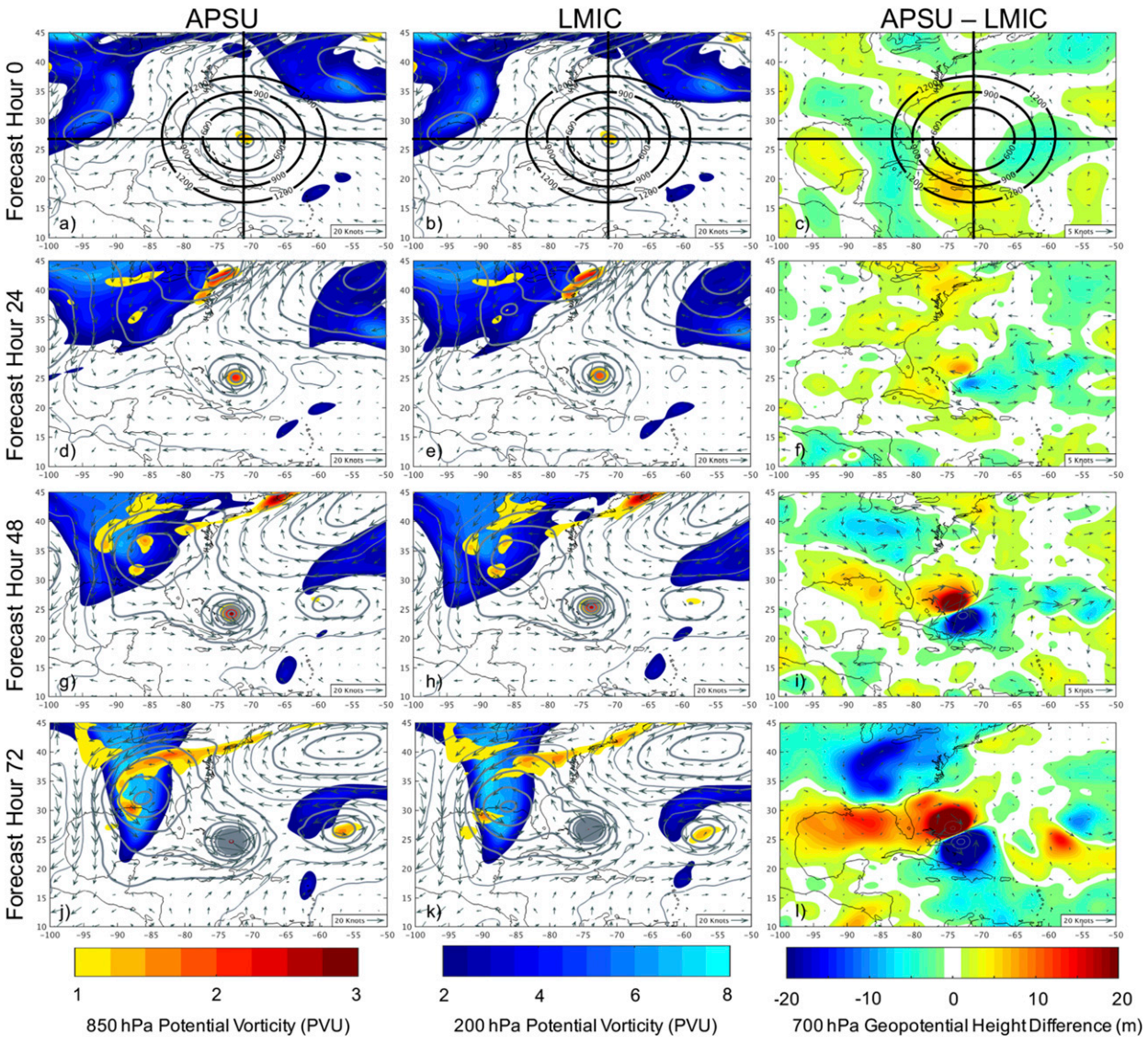

FIG. 15. Large-scale view, as in Fig. 1, but highlighting differences between (left) APSU and (middle) LMIC forecast, where 700-hPa geopotential height is contoured every 20 m. (right) The difference between APSU and LMIC, where 700-hPa geopotential height differences are colored, 700-hPa wind differences are shown as vectors, and 850-hPa PV differences are contoured every 1 PVU.

The forecasts from these APSU environment radii-relaxation sensitivity experiments are shown in Figs. 16a and 16b. As expected, because all of these sensitivity experiments utilize the same initial inner-core region, there was little to no impact on the intensity forecasts (not shown). However, significant variability occurs in the track forecasts by varying the environment relaxation radius between 300 and 1200 km (Figs. 16a,b). When the IC differences are gradually removed beyond 1200 (RE1200) and 900 km (RE900) from the initial storm center locations, the forecast tracks still make landfall on the U.S. East Coast, as in LMIC, and are nearly identical. This suggests that IC differences greater than 900 km from the initial storm center location alone are not enough to result in Joaquin's track bifurcation. However, when the ICs are relaxed starting at 600 km (RE600) from the initial storm center location, the forecast track shifts significantly eastward and does not forecast a landfall on the U.S. East Coast. These results suggest that relaxation to APSU environmental conditions outward of 900-km radius do not largely contribute to the track bifurcation in Joaquin's track, whereas IC perturbations inside of 900-km radius are clearly important in explaining the track bifurcation. As the radius of relaxation to APSU environment decreased, the position of Joaquin between 24 and 48 h

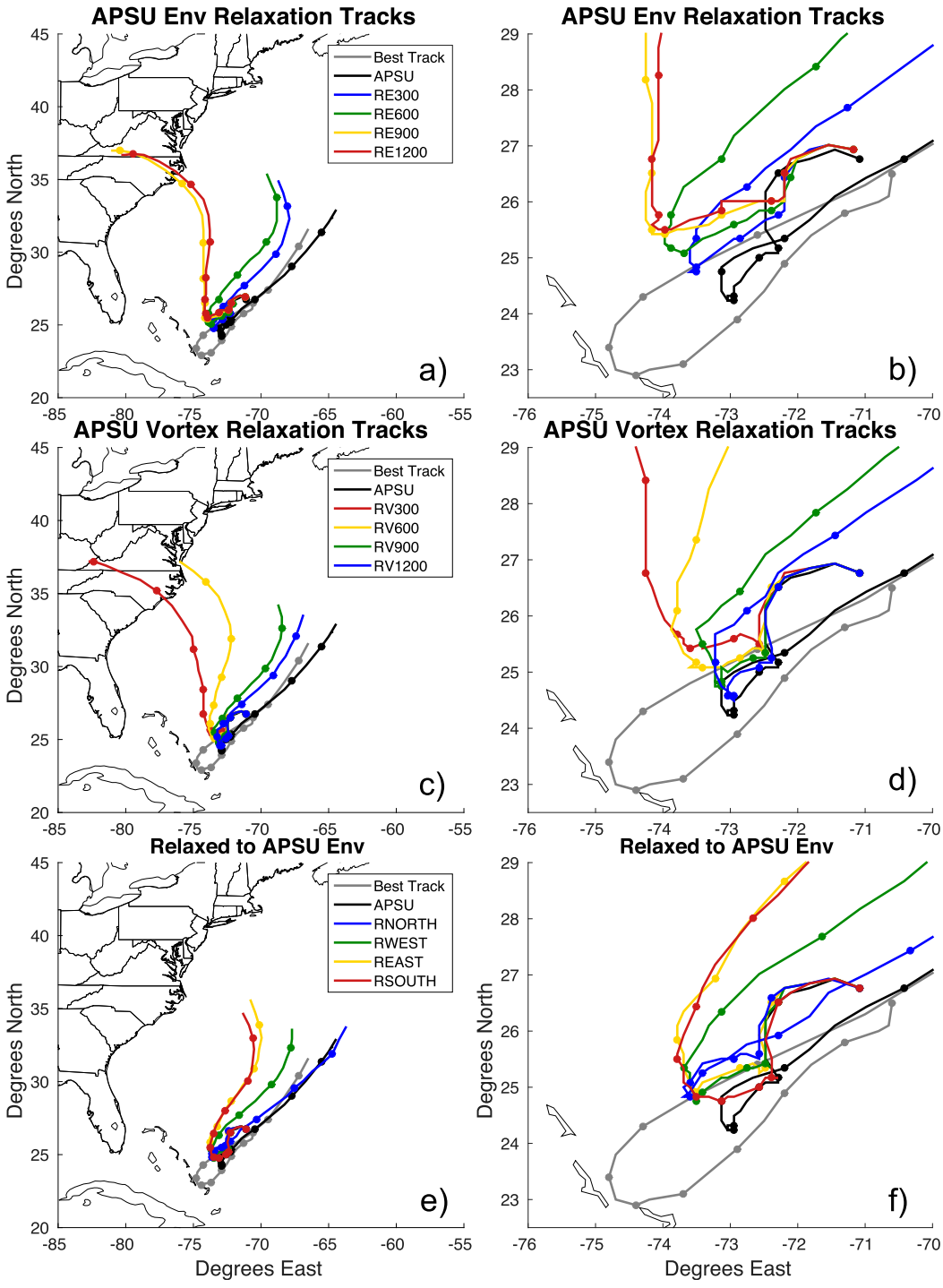

FIG. 16. (top) Forecasts for APSU environment relaxation experiments from LMIC for (a) track and (b) zoomed-in view of track divergence. (middle) Forecasts for APSU vortex relaxation experiments from LMIC for (c) track and (d) zoomed-in view of track divergence. (bottom) Forecasts for relaxation of LMIC to APSU in the north, south, east, or west relative to initial storm center location and outside 300 km for (e) track and (f) zoomed-in view of track divergence.

shifts farther to the south and better matches the actual initial motion (Fig. 16b).

To further attest this result, we also analyzed the sensitivity of relaxing LMIC to the APSU vortex at radii of 300 (RV300), 600 (RV600), 900 (RV900), and 1200 km (RV1200), with blending again done over a 300-km distance (e.g., 300–600, 600–900, 900–1200, and 1200–1500 km). By relaxing to the APSU vortex within a given radius, we are effectively removing IC differences between APSU and LMIC within that radius.

The forecasts from the APSU-vortex radii-relaxation sensitivity experiments are shown in Figs. 16c and 16d. For the experiments with IC perturbations removed within 300 (RV300) and 600 km (RV600), the forecast tracks still make landfall on the U.S. East Coast (Fig. 16c). The forecast track of RV600 is shifted east of RV300, suggesting even some impact of the region between 300 and 600 km from the initial storm center and track. However, when IC perturbations are removed within 900 km (RV900) from the initial storm center, the forecast track is now considerably farther east and does not intersect the U.S. East Coast. As in the experiments with relaxation to the APSU environment, IC differences between 600 and 900 km from the initial storm center contribute most significantly to the forecast track differences. Additionally, as the radius of relaxation to APSU vortex increased, the position of Joaquin between 24 and 48 h shifted to the south, again better matching the actual initial motion (Fig. 16d). As before, the impacts on forecast intensity from the APSU vortex relaxation radii experiments were minimal (not shown). The sensitivity of the forecasted track of Joaquin to IC differences in the near-storm environment (600–900 km from initial center) is in agreement with Majumdar et al. (2006), who demonstrated sensitivity to the near-storm environment and recommended sampling in the vicinity of storms. Harnisch and Weissmann (2010) also found greatest impact on track forecasts from assimilating dropsondes in the vicinity of the storms' outer boundary.

In addition to the eventual east–west position difference in the divergent tracks, there is also a north–south position difference that develops in the early stages of the forecast period, at ~24 h (Figs. 10a,b, 12, 15f, 16a–d). In both sets of relaxation-radii experiments, the forecasts with more southern positions over the first 24–48 h also have tracks that are farther east at the end of the forecast period (Figs. 16b,d). We generally see a similar relationship within the members of the composite groups from the real-time ensemble (Fig. 10a). If we examine the time-hodograph optimal steering flow from the APSU environment relaxation-radii experiments, using the same TC removal radii (4°) and vertical depth (850–350 hPa) (Figs. 17a,b), we observe that the forecast from RE600 is steered more southerly than the forecast from RE900 over the first 48 h. Between 60 and 96 h, RE600 km is steered more easterly than RE900. Similarly, the time-hodograph steering wind for the APSU-vortex relaxed-radii experiments (Figs. 17c,d) also show that the storms that were steered more southerly over the first 48 h (RV900 and RV1200) were subsequently steered more easterly between 48 and 96 h. Therefore, it appears that the east–west bifurcation in the forecast tracks of Joaquin may be caused by differences in the poorly captured southwestward motion of Joaquin over the first 48 h, which then influenced the zonal steering flow over the remainder of the forecast period. It is important to remember that this unusual southwestward motion was also poorly captured in most of the operational dynamical models (Berg 2016), including many of the ensemble members of the PSU WRF EnKF presented here that did correctly forecast Joaquin to head out to sea.

Returning to the large-scale differences between APSU and LMIC, the initial 700-hPa winds between 600- and 900-km radius (highlighted by the rings located at 600, 900, and 1200 km from the initial storm center) tend to be more northerly in APSU, especially north of the initial center (Figs. 15a–c). The slightly more northerly winds in this region (between 600 and 1200 km from the storm center) may have caused a more southern motion over the first 48 h. This then resulted in a more eastward motion over the remainder of the forecast as a result of zonal steering-flow differences that arose from position differences of Joaquin relative to the midlevel low pressure system over the southeastern United States.

Last, we examined the most important region (north, east, south, or west) relative to the initial location of Joaquin in causing the track bifurcation. The relaxation of LMIC is done identical to Renv (between 300 and 600 km) but is limited to the north of the initial center location for Rnorth. Everywhere south of the initial center latitude and greater than 300 km is unchanged from LMIC. The Reast, Rsouth, and Rwest experiment ICs are developed following the same methodology with blending along the latitude (Rnorth and Rsouth) or longitude (Reast and Rwest) of the initial center location. The initial inner core (the region inside of 300 km) is from APSU for all experiments.

The greatest difference from the LMIC track forecast among the various track forecasts occurs in the Rnorth experiment (Figs. 16e,f). In fact, the forecast track from the Rnorth experiment is quite similar to that of APSU. This result suggests that the northern region introduced the most significant uncertainties that subsequently lead to track bifurcation in the ensemble forecasts of Joaquin. This is not to say that IC differences to the south

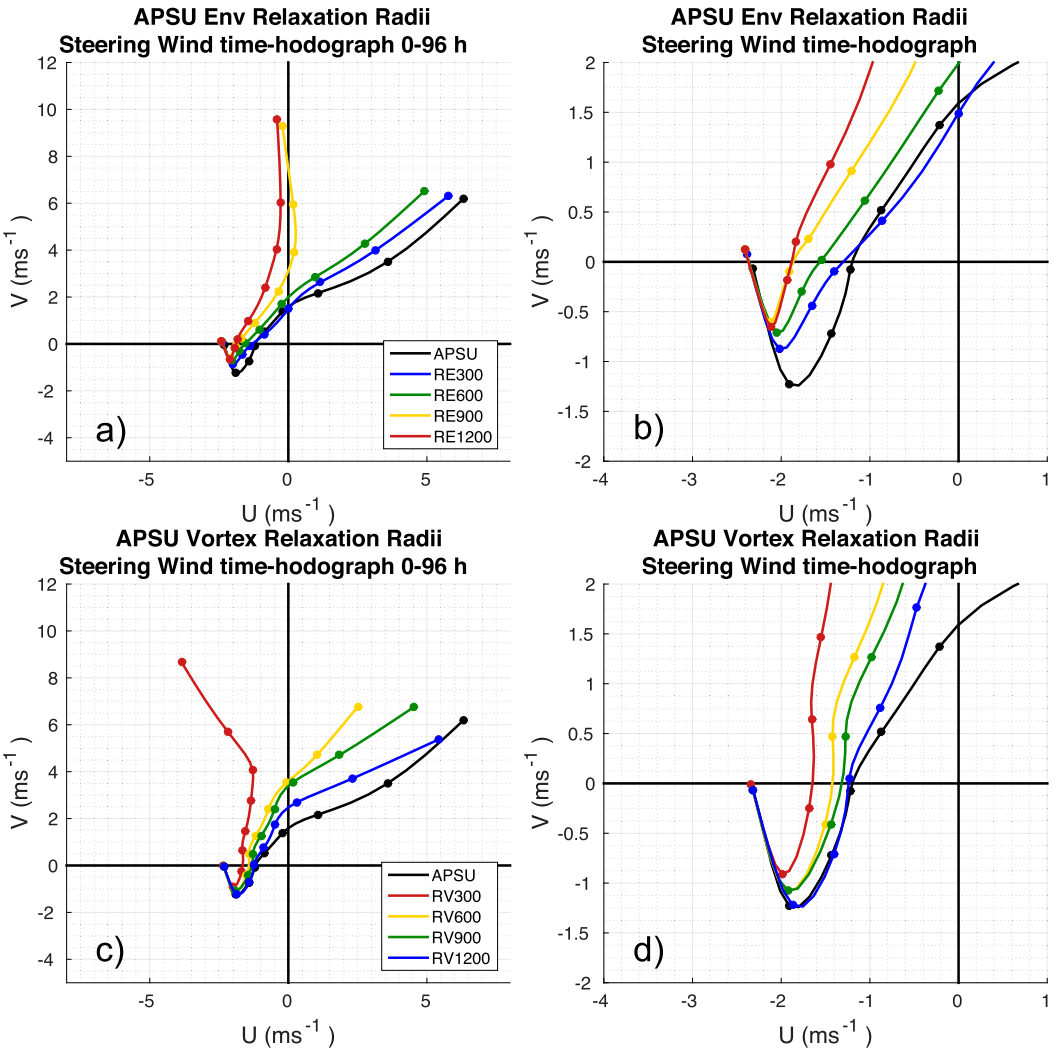

FIG. 17. Optimal steering through time for (a),(b) the APSU environment and (c),(d) the vortex initial condition relaxation radii forecasts. (b),(d) Zoomed-in view to more clearly illustrate differences leading up to the time of track divergence. Markers denote every 12 h.

(Rsouth), east (Reast), or west (Rwest) of the initial position did not have any effect on the forecast track of Joaquin, because when APSU ICs are substituted for LMICs in any of the regions, the tracks did become closer to that of APSU. The IC differences to the east (Reast) also appear to have less impact than those to the west (Rwest) on the track forecast of Joaquin, suggesting increased sensitivity to the upstream weather systems.

4. Concluding remarks

It has been shown that while the PSU WRF EnKF deterministic forecast for Hurricane Joaquin from 1200 UTC 29 September was somewhat successful, in terms of both track and intensity, the associated ensemble forecast revealed large uncertainty in both of these forecasts. Using a series of sensitivity experiments, we demonstrated that the early intensity spread was largely dominated by IC differences within 300 km from the vortex center. More specifically, the intensity spread was strongly controlled by initial intensity differences, with the stronger initial members generally intensifying and the weakest members not intensifying at all. The track spread, on the other hand, was largely dominated by IC differences outside of 300 km from the vortex position and not from initial position differences or initial inner-core differences.

In the scenario where no inner-core uncertainty exists (Rcore), large-scale environment IC errors (greater than 300 km from the initial vortex position) result in

intensity forecast spread growth. However, IC differences to the storm's inner-core region (within 300 km from the initial center) are still the leading source of intensity forecast errors at early forecast times, and improved inner-core ICs are needed to reduce intensity spread any further for the time shown here. Even if all IC error to the environment is removed (Renv), the intensity forecast spread is nearly identical to that when IC error exists everywhere (CNTL), demonstrating that without improvement to the ICs within the inner-core region, this intensity forecast will not improve. As a consequence, these results strongly indicate the current need for better observations and data assimilation methods to reduce inner-core IC uncertainty if we want to see significant intensity forecast improvements. This is especially true when aircraft observations are not available like the time shown here and initial intensity spread is large.

Further examination of the track bifurcation in the ensemble, by constructing two composite groups separating members that incorrectly made landfall on the U.S. East Coast (Left) and members that correctly tracked out to sea (Right), revealed no obvious intensity relationship to the ensemble tracks since both the Left and Right composite groups contain members that intensify into major hurricanes and members that do not intensify. Through examining the steering winds, we showed that the Left composite group members generally had a stronger positive meridional steering wind over the first 24 h, which resulted in a north–south position difference in Joaquin between the groups. After 24 h, the Right members generally had a stronger positive zonal steering wind. We also examined the time-hodograph steering wind for the composite groups and showed that the Right members generally were located more to the south after the first 24 h and then were steered farther east, out to sea, by stronger positive zonal steering flow. The intensity differences were not a major factor in the track bifurcation because uncertainties in the low to midlevels (~700 hPa) appeared to most largely contribute to steering differences, and storms of all intensity appear steered, at least partly, by this region.

Through the mean composite group IC forecast, we showed the importance of the position of Joaquin relative to the mid- to upper-level low pressure system over the southeast United States on the forecast track. We then demonstrated the importance of IC differences between 600 and 900 km from the initial storm center in the track bifurcation by gradually decreasing the radii from the storm center at which the environment is identical to APSU or by gradually increasing the size of the vortex that is identical to APSU. Additionally, the differences in this region were not found to be associated with a single specific large-scale dynamical feature. Finally, we demonstrated that when IC differences north of the initial storm center are removed, the forecast track is most similar to that of APSU.

The regions of IC differences most sensitive on the track forecasts of Joaquin differ from those found in Munsell and Zhang (2014) for Hurricane Sandy (2012), which showed that Sandy was sensitive to IC differences in the mean tropical flow rather than in the midlatitude environment, further demonstrating that the regions of greatest sensitivity can vary for each storm. Additionally, while large track uncertainty of recurving TCs are often thought to be caused by differences in midlatitude troughs, the results of this study and others (e.g., Majumdar et al. 2006; Harnisch and Weissmann 2010; Munsell and Zhang 2014; Torn et al. 2015; Bassill 2015) demonstrate that large ensemble track spread can result from IC differences to the near-storm environment and do not require differences in the ICs of midlatitude troughs, although they can also be important.

Acknowledgments. This research is partially supported by NASA Grant NNX15AM84G, ONR Grants N000141512298 and N000141410062, and NOAA under the Hurricane Forecast Improvement Program (HFIP). Erin Munsell is supported by a NASA Postdoctoral Program Fellowship at GSFC, which is supported by USRA through a contract with NASA. Computing was conducted at the Texas Advanced Computing Center (TACC). All modeling and analysis dataset are saved at TACC and can be made freely available upon request. The authors are grateful to the anonymous reviewers for their comments on the earlier version of this manuscript.

REFERENCES

Barker, D. M., W. Huang, Y. R. Guo, A. J. Bourgeois, and Q. N. Xiao, 2004: A three-dimensional variational data assimilation system for MM5: Implementation and initial results. *Mon. Wea. Rev.*, **132**, 897–914, https://doi.org/10.1175/1520-0493(2004)132<0897:ATVDAS>2.0.CO;2.

Bassill, N. P., 2015: An analysis of the operational GFS simplified Arakawa Schubert parametrization within a WRF framework: A Hurricane Sandy (2012) long-term track forecast perspective. *J. Geophys. Res. Atmos.*, **120**, 378–398, https://doi.org/10.1002/2014JD022211.

Berg, R., 2016: Tropical cyclone report: Hurricane Joaquin (AL112015). National Hurricane Center Tech. Rep., 36 pp.

Cangialosi, J., and J. Franklin, 2016: National Hurricane Center forecast verification report: 2015 hurricane season. NOAA Rep., 69 pp.

Chan, J. C. L., 2005: The physics of tropical cyclone motion. *Annu. Rev. Fluid Mech.*, **37**, 99–128, https://doi.org/10.1146/annurev.fluid.37.061903.175702.

——, and K. K. Li, 2005: Ensemble forecasting of tropical cyclone motion using a barotropic model. Part III: Combining perturbations of the environment and the vortex. *Meteor. Atmos. Phys.*, **90**, 109–126, https://doi.org/10.1007/s00703-004-0092-9.

Chen, H., and D. Zhang, 2013: On the rapid intensification of Hurricane Wilma (2005). Part II: Convective bursts and the

upper-level warm core. *J. Atmos. Sci.*, **70**, 146–162, https://doi.org/10.1175/JAS-D-12-062.1.

——, and S. G. Gopalakrishan, 2015: A study of the asymmetric rapid intensification of Hurricane Earl (2010) using the HWRF system. *J. Atmos. Sci.*, **72**, 531–550, https://doi.org/10.1175/JAS-D-14-0097.1.

Cheung, K. K., and J. C. L. Chan, 1999a: Ensemble forecasting of tropical cyclone motion using a barotropic model. Part I: Perturbations of the environment. *Mon. Wea. Rev.*, **127**, 1229–1243, https://doi.org/10.1175/1520-0493(1999)127<1229:EFOTCM>2.0.CO;2.

——, and ——, 1999b: Ensemble forecasting of tropical cyclone motion using a barotropic model. Part II: Perturbations of the vortex. *Mon. Wea. Rev.*, **127**, 2617–2640, https://doi.org/10.1175/1520-0493(1999)127<2617:EFOTCM>2.0.CO;2.

Dong, K., and C. J. Neumann, 1986: The relationship between tropical cyclone motion and environmental geostrophic flows. *Mon. Wea. Rev.*, **114**, 115–122, https://doi.org/10.1175/1520-0493(1986)114<0115:TRBTCM>2.0.CO;2.

Emanuel, K., and F. Zhang, 2016: On the predictability and error sources of tropical cyclone intensity forecasts. *J. Atmos. Sci.*, **73**, 3739–3747, https://doi.org/10.1175/JAS-D-16-0100.1.

——, and ——, 2017: The role of inner-core moisture in tropical cyclone predictability and practical forecast skill. *J. Atmos. Sci.*, **74**, 2315–2324, https://doi.org/10.1175/JAS-D-17-0008.1.

Fiorino, M., and R. L. Elsberry, 1989: Some aspects of vortex structure related to tropical cyclone motion. *J. Atmos. Sci.*, **46**, 975–990, https://doi.org/10.1175/1520-0469(1989)046<0975:SAOVSR>2.0.CO;2.

Galarneau, T. J., and C. A. Davis, 2013: Diagnosing forecast errors in tropical cyclone motion. *Mon. Wea. Rev.*, **141**, 405–430, https://doi.org/10.1175/MWR-D-12-00071.1.

Gamache, J. F., F. D. Marks Jr., and F. Roux, 1995: Comparison of three airborne Doppler sampling techniques with airborne in situ wind observations in Hurricane Gustav (1990). *J. Atmos. Oceanic Technol.*, **12**, 171–181, https://doi.org/10.1175/1520-0426(1995)012<0171:COTADS>2.0.CO;2.

George, J. E., and W. M. Gray, 1976: Tropical cyclone motion and surrounding parameter relationships. *J. Appl. Meteor.*, **15**, 1252–1264, https://doi.org/10.1175/1520-0450(1976)015<1252:TCMASP>2.0.CO;2.

Hamill, T. M., J. S. Whitaker, M. Fiorino, and S. G. Benjamin, 2011: Global ensemble predictions of 2009's tropical cyclones initialized with an ensemble Kalman filter. *Mon. Wea. Rev.*, **139**, 668–688, https://doi.org/10.1175/2010MWR3456.1.

Harnisch, F., and M. Weissmann, 2010: Sensitivity of typhoon forecasts to different subsets of targeted dropsonde observations. *Mon. Wea. Rev.*, **138**, 2664–2680, https://doi.org/10.1175/2010MWR3309.1.

Komaromi, W. A., and S. J. Majumdar, 2014: Ensemble-based error and predictability metrics associated with tropical cyclogenesis. Part I: Basinwide perspective. *Mon. Wea. Rev.*, **142**, 2879–2898, https://doi.org/10.1175/MWR-D-13-00370.1.

——, ——, and E. D. Rappin, 2011: Diagnosing initial condition sensitivity of Typhoon Sinlaku (2008) and Hurricane Ike (2008). *Mon. Wea. Rev.*, **139**, 3224–3242, https://doi.org/10.1175/MWR-D-10-05018.1.

Landsea, C. W., 1993: A climatology of intense (or major) Atlantic hurricanes. *Mon. Wea. Rev.*, **121**, 1703–1713, https://doi.org/10.1175/1520-0493(1993)121<1703:ACOIMA>2.0.CO;2.

Magnusson, L., J. Bidlot, S. T. Lang, A. Thorpe, N. Wedi, and M. Yanmaguchi, 2014: Evaluation of medium-range forecasts of Hurricane Sandy. *Mon. Wea. Rev.*, **142**, 1962–1981, https://doi.org/10.1175/MWR-D-13-00228.1.

Majumdar, S. J., S. D. Aberson, C. H. Bishop, R. Buizza, M. S. Peng, and C. A. Reynolds, 2006: A comparison of adaptive observing guidance for Atlantic tropical cyclones. *Mon. Wea. Rev.*, **134**, 2354–2372, https://doi.org/10.1175/MWR3193.1.

Munsell, E. B., and F. Zhang, 2014: Prediction and uncertainty of Hurricane Sandy (2012) explored through a real-time cloud-permitting ensemble analysis and forecast system assimilating airborne Doppler radar observations. *J. Adv. Model. Earth Syst.*, **6**, 38–58, https://doi.org/10.1002/2013MS000297.

——, ——, and D. P. Stern, 2013: Predictability and dynamics of a nonintensifying tropical storm: Erika (2009). *J. Atmos. Sci.*, **70**, 2505–2524, https://doi.org/10.1175/JAS-D-12-0243.1.

——, ——, J. A. Sippel, S. A. Braun, and Y. Weng, 2017: Dynamics and predictability of the intensification of Hurricane Edouard (2014). *J. Atmos. Sci.*, **74**, 573–595, https://doi.org/10.1175/JAS-D-16-0018.1.

Rios-Berrios, R., and R. Torn, 2016: An ensemble approach to investigate tropical cyclone intensification in sheared environments. Part I: Katia (2011). *J. Atmos. Sci.*, **73**, 71–93, https://doi.org/10.1175/JAS-D-15-0052.1.

Sippel, J. A., and F. Zhang, 2010: Factors affecting the predictability of Hurricane Humberto (2007). *J. Atmos. Sci.*, **67**, 1759–1778, https://doi.org/10.1175/2010JAS3172.1.

——, S. A. Braun, and C.-J. Shie, 2011: Environmental influences on the strength of Tropical Storm Debby (2006). *J. Atmos. Sci.*, **68**, 2557–2581, https://doi.org/10.1175/2011JAS3648.1.

Skamarock, W. C., and Coauthors, 2008: A description of the Advanced Research WRF version 3. NCAR Tech. Note NCAR/TN-475+STR, 113 pp., https://doi.org/10.5065/D68S4MVH.

Tang, B., and K. Emanuel, 2010: Midlevel ventilation's constraint on tropical cyclone intensity. *J. Atmos. Sci.*, **67**, 1817–1830, https://doi.org/10.1175/2010JAS3318.1.

Tao, D., and F. Zhang, 2014: Effect of environmental shear, sea-surface temperature, and ambient moisture on the formation and predictability of tropical cyclones: An ensemble-mean perspective. *J. Adv. Model. Earth Syst.*, **6**, 384–404, https://doi.org/10.1002/2014MS000314.

——, and ——, 2015: Effects of vertical wind shear on the predictability of tropical cyclones: Practical versus intrinsic limit. *J. Adv. Model. Earth Syst.*, **7**, 1534–1553, https://doi.org/10.1002/2015MS000474.

Torn, R. D., 2016: Evaluation of atmospheric and ocean initial condition uncertainty and stochastic exchange coefficients on ensemble tropical cyclone intensity forecasts. *Mon. Wea. Rev.*, **144**, 3487–3506, https://doi.org/10.1175/MWR-D-16-0108.1.

——, and D. Cook, 2013: The role of vortex and environment errors in genesis forecasts of Hurricanes Danielle and Karl (2010). *Mon. Wea. Rev.*, **141**, 232–251, https://doi.org/10.1175/MWR-D-12-00086.1.

——, J. S. Whitaker, P. Pegion, T. M. Hamill, and G. J. Hakim, 2015: Diagnosis of the source of GFS medium-range track errors in Hurricane Sandy (2012). *Mon. Wea. Rev.*, **143**, 132–152, https://doi.org/10.1175/MWR-D-14-00086.1.

Velden, C. S., 1993: The relationship between tropical cyclone motion, intensity, and the vertical extent of the environmental steering layer in the Atlantic basin. Preprints, *20th Conf. on Hurricanes and Tropical Meteorology*, San Antonio, TX, Amer. Meteor. Soc., 31–34.

——, and L. M. Leslie, 1991: The basic relationship between tropical cyclone intensity and the depth pf the environmental steering layer in the Australian region. *Wea. Forecasting*, **6**, 244–253, https://doi.org/10.1175/1520-0434(1991)006<0244:TBRBTC>2.0.CO;2.

Weng, Y., and F. Zhang, 2012: Assimilating airborne Doppler radar observations with an ensemble Kalman filter for convection-permitting hurricane initialization and prediction: Katrina (2005). *Mon. Wea. Rev.*, **140**, 841–859, https://doi.org/10.1175/2011MWR3602.1.

——, and ——, 2016: Advances in convection-permitting tropical cyclone analysis and prediction through EnKF assimilation of reconnaissance aircraft observations. *J. Meteor. Soc. Japan*, **94**, 345–358, https://doi.org/10.2151/jmsj.2016-018.

Wu, C., and K. A. Emanuel, 1995: Potential vorticity diagnostics of hurricane movement. Part II: Tropical Storm Ana (1991) and Hurricane Andrew (1992). *Mon. Wea. Rev.*, **123**, 93–109, https://doi.org/10.1175/1520-0493(1995)123<0093:PVDOHM>2.0.CO;2.

Zhang, F., and J. A. Sippel, 2009: Effects of moist convection on hurricane predictability. *J. Atmos. Sci.*, **66**, 1944–1961, https://doi.org/10.1175/2009JAS2824.1.

——, and D. Tao, 2013: Effects of vertical wind shear on the predictability of tropical cyclones. *J. Atmos. Sci.*, **70**, 975–983, https://doi.org/10.1175/JAS-D-12-0133.1.

——, and Y. Weng, 2015: Predicting hurricane intensity and associated hazards: A five-year real-time forecast experiment with assimilation of airborne Doppler radar observations. *Bull. Amer. Meteor. Soc.*, **96**, 25–33, https://doi.org/10.1175/BAMS-D-13-00231.1.

Zhang, Z., and T. N. Krishnamurti, 1997: Ensemble forecasting of hurricane tracks. *Bull. Amer. Meteor. Soc.*, **78**, 2785–2795, https://doi.org/10.1175/1520-0477(1997)078<2785:EFOHT>2.0.CO;2.